Structural and reflective characteristics of multilayers for 6.x nm wavelength

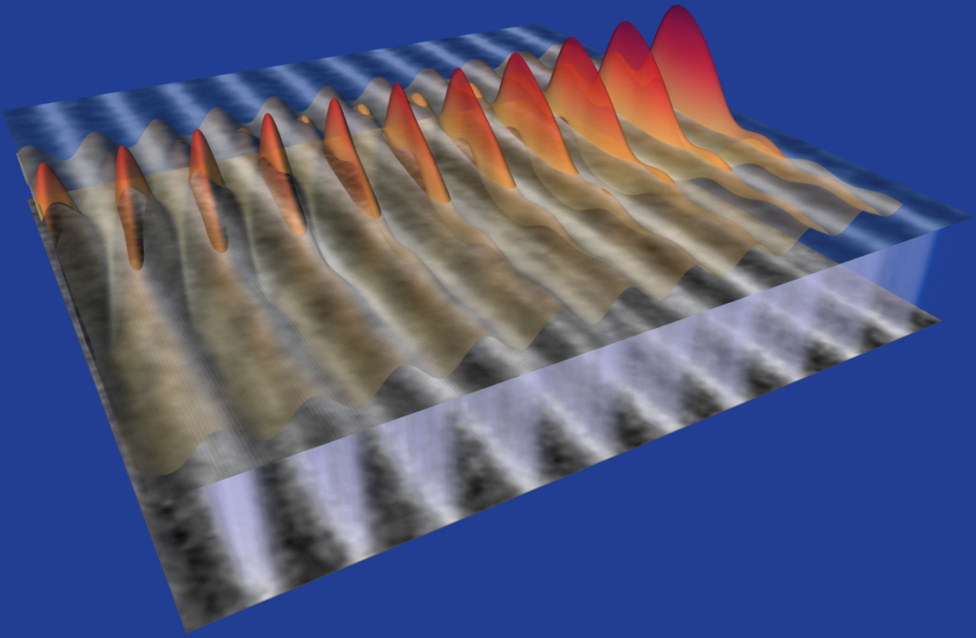

Igor A. Makhotkin

Structural and reflective characteristics of multilayers for 6.x nm wavelength

Igor A. Makhotkin

Ph.D. committee

Chairman:	
prof.dr. G. van der Steenhoven	University of Twente
Secretary:	
prof.dr. G. van der Steenhoven	University of Twente
Promotor:	
prof.dr. F. Bijkerk	University of Twente FOM Institute DIFFER
Assistant promotor:	
dr. E. Louis	FOM Institute DIFFER University of Twente
Members:	
prof.dr.ir. J.P.H. Benschop	ASML University of Twente
prof.dr.ir. A. Brinkman	University of Twente
prof.dr. K.J. Boller	University of Twente
prof.dr.ir. B. Poelsema	University of Twente
prof.dr. B. Dam	Delft University of Technology

Cover: Transmission electron microscope image of a La/B-based multilayer mirror that is merged with the calculated electromagnetic field inside this multilayer when used in Bragg reflection conditions.

STRUCTURAL AND REFLECTIVE CHARACTERISTICS OF MULTILAYERS FOR 6.X NM WAVELENGTH

PROEFSCHRIFT

ter verkrijging van de graad van doctor
aan de Universiteit Twente, op gezag van
de rector magnificus, prof. dr. H. Brinksma,
volgens besluit van het College voor Promoties
in het openbaar te verdedigen op
donderdag 31 oktober 2013
om 14:45 uur

door

Igor Alexandrovich Makhotkin
geboren op 28 juli 1985
te Moskou, Rusland

Dit proefschrift is goedgekeurd door de promotor:

Prof.dr. F. Bijkerk

en assistent promotor

dr. E. Louis

ISBN: 978-94-6191-912-0

This thesis is based on following publications:

Chapter 2.2: The introduction section of: S.N. Yakunin, I.A. Makhotkin, C. Nikolayev, M.A. Chuev, E.M. Pashaev, E. Zoethout, E. Louis, R.W.E. van de Kruijs, M.V. Kovalchuk and F. Bijkerk, “The simultaneous analysis of grazing incidence X-ray reflectivity and normal incidence extreme ultraviolet reflection”, in preparation.

Chapter 3: Makhotkin, I. A., Zoethout, E., Louis, E., Yakunin, A. M., Müllender, S., and Bijkerk, F., "Spectral properties of La/B - based multilayer mirrors near the boron K absorption edge.", *Opt. Express*, 20(11), 11778-11786, 2012.

Chapter 4: Makhotkin, I. A., Zoethout, E., Louis, E., Yakunin, A. M., Müllender, S., and Bijkerk, F., "Wavelength selection for multilayer coatings for lithography generation beyond extreme ultraviolet.", *JM3 letters*, 11(4), 040501-1-040501-3, 2012.

Chapter 5: I. A. Makhotkin, E. Zoethout, R.W.E. van de Kruijs, S. N. Yakunin, E. Louis, A. M. Yakunin, S. Müllender and F. Bijkerk, “Short period La/B and LaN/B multilayer mirrors for ~6.8 nm wavelength.”, submitted to Optics Express.

Chapter 6: Makhotkin, I. A., Louis, E., van de Kruijs, R. W. E., Yakshin, A. E., Zoethout, E., Seregin, A. Y., Tereschenko, E. Y., Yakunin, S. N., and Bijkerk, F., "Determination of the density of ultrathin La films in La/B_4C layered structures using X-ray standing waves.", *physica status solidi (a)*, 208(11), 2597-2600, (2011).

Chapter 7: S.N. Yakunin, I.A. Makhotkin, M.A. Chuev, E.M. Pashaev, E. Zoethout, E. Louis, R.W.E. van de Kruijs, S.Yu. Seregin, I.A. Subbotin, D.V. Novikov, F. Bijkerk and M.V. Kovalchuk, “Model independent X-ray standing wave analysis of periodic multilayer structures”, submitted to Phys. Rev. B .

This work is part of the project ‘Multilayer Optics for Lithography Beyond the Extreme Ultraviolet Wavelength Range’, carried out with support of the Dutch Technology Foundation (STW), in collaboration with Carl Zeiss SMT and ASML.

Contents

1 Introduction

1.1 Optical elements of EUV photolithography

Photolithography is used in semiconductor industry for the creation of 2D and 3D patterns of integrated circuits, e.g. processor or memory chips. The continued demand for the increase of computer power and processor speed requires an increase of the amount and density of electronic components, like transistors, on integrated circuits. This can be achieved by decreasing the size of the electronic features. For the lithographic process, this means a continuous requirement to improve the minimal printable feature size, which is determined by the resolution. This, in turn, is limited by the well-known Rayleigh criterion [1]: $\Delta \sim \lambda / NA$, where Δ is minimal printable feature size and NA is the numerical aperture of the optical system and λ the working wavelength. Therefore the resolution can be improved, either by reducing the wavelength or increasing the numerical aperture of the projection optics. Another important parameter for the lithography industry is the depth of focus (DOF) of the optical system, because the value of the DOF determines the required wafer alignment accuracy. The value of the DOF increases linearly with the wavelength reduction, which is favourable for the production process.

Today, 193 nm photolithography is used for mass production. Using water immersion projection lenses to allow an increase of the NA, and off-axis illumination and multiple patterning, it was possible to resolve features of 32 nm using 193 nm light [2]. However, such a complicated process unavoidably leads to higher production costs and further resolution increase requires the reduction of the operational wavelength. This wavelength generally determines the design of the lithography equipment including the type of source, optics and photosensitive resist.

For a wavelength below 100 nm classical transmissive lenses are not effective because of high absorption and low refraction properties. Therefore reflective optics have to be used. Single layer reflective coatings can be used only as grazing incidence mirrors for incidence angles within the total external reflection regime where the reflectivity is close to unity. However at more normal angles of incidence their reflection coefficient is extremely small, limiting their application. The solution can be found in the application of a periodic multilayer mirror where high reflectance is achieved because of constructive interference of waves reflected from all individual layer interfaces. The first realistic candidate wavelength lower than 193 nm for which a sufficiently high reflectance can be achieved in combination with a large DOF is around 13.5 nm, in the so-called extreme ultraviolet wavelength (EUV) range. For this wavelength Mo/Si multilayer mirrors are used with typical reflection close to 70%. The record value reported for near normal incidence reflectivity is 70.3% [3].

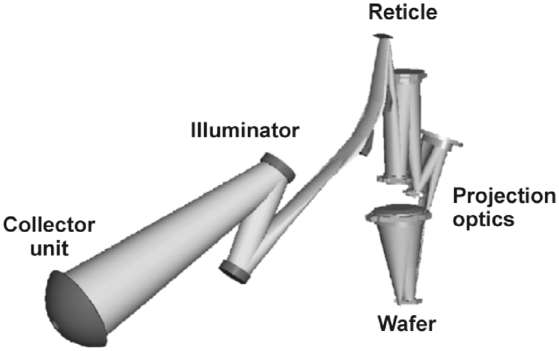

Figure 1.1 Optical scheme for 13.5 nm lithography.

An example of an all reflective optical scheme for 13.5 nm photolithography is presented in Figure 1.1 containing 10 multilayer mirrors. Each mirror has its own specification, but all of them should be coated with a state-of-the-art multilayer stack, enabling the highest possible transmission of the optical system. This transmission is determined by two parameters: the peak reflectance value and the bandwidth of the reflectivity curve, the latter depending on the number of interfaces contributing to the reflectance. The peak reflectance is the dominant parameter, making the research on multilayer stacks of vital importance for photolithography, making it important for the entire semiconductor industry. The first EUV tools have already been delivered to customers. An image with a resolution of 13 nm in a single exposure mode using 13.5 nm light, i.e. without additional resist process steps, was demonstrated with the NXE:3100 tool [4].

Photolithography using an even shorter wavelength of ~6.x nm (the value of x still has to be determined by the industry), has the potential to be a possible successor of the currently introduced EUV lithography using 13.5 nm. Furthermore, the 6.x nm process in general will allow working with a low NA value of 0.3. This will result in an increased DOF compared to what is achievable with the larger, 13.5 nm wavelength.

1.2 6.x nm photolithography

Transition from 13.5 to 6.x nm photolithography will require complex revision of all elements of the lithography machine, depending on the wavelength: the radiation source, optics and photoresist. Currently, only few aspects regarding lithography using 6.x nm light are determined. Research in optics and radiation sources is ongoing, in parallel and independently, but the selection of the exact wavelength should be done in close collaboration between optics and source researchers. A brief introduction of possible sources and their influence on the optics is given in section 1.2.1. An introduction to the optics development for 6.x nm wavelength is presented in section 1.2.2.

1.2.1 Light source for 6.x nm photolithography

To select the wavelength for the next generation lithography, the reflectance characteristics of optical column should be compared to the emission spectrum of the possible light sources. For 13.5 nm lithography the radiation source is based on light emission of a laser produced (LPP) Sn plasma. For a number of reasons [5] Sn is not a viable material for a 6.x nm light source. Pioneering work on possible source materials for 6.x nm [6] states two materials: Tb and Gd. They have high intensity emission with the highest intensities at 6.5 and 6.9 nm wavelength correspondingly. However, it is estimated [7] that to generate 1 kW of radiated power from a Gd plasma a 160 kW CO_2 laser source is required. This is more power than required for a 13.5 nm source and makes a laser produced plasma source development even more challenging. By consequence, it can be expected that problems typical for LPP sources, such as contamination of optics by plasma debris and parasitic IR reflection by the collector, may also be more substantial.

An alternative source type considered is a free electron laser (FEL), as discussed by Türke [8]. With existing technology, a dedicated FEL was claimed to provide sufficient power, unlike an LPP to be optimized for any required wavelength. Another advantage of a FEL is that it produces “clean” photons: the source will not create debris or long wavelength radiation outside the EUV range. However, a FEL creates ultra short, high flux coherent pulses in a very a small beam. Additionally, a FEL is a complicated multi-component facility that requires a large floor space.

While the wavelength selection will just slightly influence the coating design for the optics, the radiation source will most likely determine the entire collector mirror design. For LPP sources there are two options available: normal incidence (NIC) and grazing incidence (GIC) collectors [9]. The NIC is based on a multilayer stack allowing high acceptance angles, thus a large collection angle and a high efficiency. However the internal structure of the multilayer coating is likely to be sensitive to high thermal loads and the hostile environment in the collector module of the lithography equipment. This, particularly with the high flux density of the incidence beam could limit the lifetime of a NIC. A GIC is based on total external reflection so its efficiency depends only on the quality of the surface. Because of the grazing incidence condition the flux density for a GIC is lower than for a NIC. The simple coating design and lower thermal load makes the GIC less vulnerable then a NIC. The high peak power density of FEL pulses may cause multilayer damage as well [10, 11]. This effect would be strongly reduced when a GIC is used because of the much larger area. In addition, collector optics for a FEL will have to enlarge the beam footprint and destroy its coherency to be acceptable for the rest of the optical scheme. Regardless the collector design, projection optics and part of illumination optics in any case are based on multilayer mirrors.

1.2.2 Optics

The periodic multilayer [12, 13] consisting of optically contrasting layers, forms a one dimensional lattice that has diffraction properties similar to natural crystals. As such it can be used as a reflective coating based on Bragg reflection. One layer[14], “the reflector”, should have high refraction, as normally found in high density materials. The other layer, “the spacer”, should have the lowest possible refraction for a selected wavelength, normally found in low density materials. Both layers should have low absorption for a maximum number of interfaces to contribute to the reflectance. The highest optical contrast for a wavelength above 6.6 nm theoretically can be achieved with a La/B multilayer

[15, 16]. Boron is the most suitable material for the spacer layer because the wavelength is just above its K absorption edge around 6.6 nm. La has a relatively low absorption and high reflectance at 6.x nm wavelength, making it the best candidate material for the reflector layer.

The thickness of a bi-layer, the multilayer period *D*, in a periodic multilayer can be optimized for the reflectance of a selected wavelength λ at a selected angle between incidence beam and surface normal θ according to well-known Bragg law:

$$m\lambda = 2\mathrm{D}\cos\theta\sqrt{1-\frac{2\delta}{\cos^2\theta}}\ , \qquad (1.1)$$

where $\delta = \frac{d_r\delta_r + d_s\delta_s}{\mathrm{D}}$ is the averaged refractive index of the multilayer, *D* is the thickness of a bi-layer and index *'r'* is indicative for the reflector and *'s'* for the spacer layers. Most of the mirrors in the 13.5 nm lithography application are designed to be used close to normal incidence conditions. As a possible successor, 6.x nm lithography is likely to inherit the optics design for 13.5 nm lithography. According to Bragg's law Eq. (1.1) the period of the multilayer mirror for normal incidence reflection of 6.6 nm wavelength is approximately 3.3 nm. This makes the requirements for interface conditions extremely hard to achieve. The first experiments with La/B_4C [17, 18] multilayers have shown a huge difference between theoretical and measured reflectivity values. Intermixing of a large part of the total bi-layer thickness is considered to be the major cause of the low reflectivity. Passivation of the layers could reduce the intermixing. It was shown that nitridation of La increases the reflectivity [15] up to 41% at 6.7 nm. This is still considerably lower that the theoretically predicted reflectance of 80%. However, no structural research was done to understand the origin of the reflectivity losses of La/B_4C and LaN/B_4C multilayer mirrors.

The current thesis addresses the baseline analysis of optical (chapters 3 and 4) and structural properties (chapters 5 and 7) of La/B-based multilayer coatings. Generally we use the words 'La/B-based' as a collective noun for La/B, La/B_4C, LaN/B, LaN/B_4C and LaN/BN studied in different stages of the research discussed in this thesis. In parallel to this research, two major steps were taken to maximize the multilayer reflectivity. Firstly the traditionally used B_4C was replaced with optically favourable B and secondly the nitridation of La was optimized. It resulted in the deposition of a 175 period LaN/B multilayer mirror with a world record normal incidence reflectivity of 57% at 6.6 nm (chapter 5).

The understanding of the reflectivity behaviour of multilayers is impossible without adequate analytical tools. To support the multilayer research techniques like grazing incidence X-ray reflectivity (chapter 2) and X-ray standing wave analysis (described in chapters 6 and 7) were extended to periodic multilayers with ultrathin periods and large interface layer thicknesses.

1.3 Outline

The description of experimental setup, used for the deposition of multilayer structures is presented in chapter 2. The formalism used for the analysis of grazing incidence X-ray reflectivity data optimized for the multilayer mirrors with ultrathin periods is also described in chapter 2.

In chapter 3, the research focuses on the analysis of the optical properties of La/B based multilayer mirrors. In this chapter the theoretical and experimental studies of the reflective spectrum of 50 period LaN/B_4C and LaN/B multilayer mirrors are discussed. The goal was to understand the reflectivity behaviour of these multilayers in the wavelength range between 6.6 and 7.0 nm. We have evaluated the validity of the available optical constants for the simulation of B-based multilayer mirror reflectivity in the vicinity of boron K_α absorption edge.

To get an indication of the optical throughput of a La/B and La/B_4C coated optical column, the transmission of a perfect 10 mirror system has been calculated using measured optical constants for B and B_4C. The results are presented in chapter 4. To check the actual state of the art multilayer deposition process, 150 period LaN/B_4C multilayer mirrors were deposited and analyzed. The model reflectivity spectrum of the perfect optical system and the real multilayer reflectivity are compared to the emission spectrum of possible plasma based EUV light sources to find the best source-optics match.

The potential of La-B as a material combination is experimentally evaluated by reducing the impact of the interface imperfections on the multilayer reflectivity. The research presented in chapter 5 shows that in this case close to theoretical reflectivity value can be achieved. The current state of the deposition process for LaN/B multilayer mirrors was analyzed by comparing two promising ways of La nitridation: N-ion post treatment of every La layer and reactive sputtering of La in a N_2 atmosphere.

In parallel to the research on the optical properties we have performed a multi-parametrical optimization of the deposition of LaN/B and LaN/B_4C multilayer stacks in order to increase the multilayer reflectivity. The optimization of the deposition process requires adequate feedback on modifications in the structure and composition of the layers. However, the analysis of the structure of short period La/B based multilayers is complicated because the thickness of the interface layers is comparable to the layer thickness. In these conditions typical analysis techniques, like grazing incidence hard X-ray reflection, do not show sufficient sensitivity. Therefore we carried out simultaneous analysis of normal incidence EUV and grazing incidence hard X-ray reflectivity data by fitting them to our model.

In most multilayer analysis methods, the density of the materials in the layers cannot uniquely be determined since density and layer thickness are two coupled parameters. In chapter 6 the application of a novel X-ray Standing Waves (XSW) technique is discussed to analyze the density of the ultrathin La and LaN layers.

Additionally, the application of another XSW technique for non-destructive reconstruction of the atomic profile in periodic multilayers is discussed in chapter 7. The application of the XSW technique is limited by the complicity of the experimental data analysis. To overcome this, chapter 7 offers a mode independent approach to the analysis of fluorescence radiation excited by the XSW that is formed in Bragg reflection conditions.

1.4 References

1. Born, M. and E. Wolf, *Principles of optics*. 1999: Cambridge University Press.
2. Wagner, C. and N. Harned, *EUV lithography: Lithography gets extreme*. Nat Photon. **4**(1): p. 24-26.
3. Bosgra, J., et al., Structural properties of subnanometer thick Y layers in extreme ultraviolet multilayer mirrors. Appl. Opt. **51**(36): p. 8541-8548.
4. asml.com
5. Banine, V., et al., Opportunity to extend EUV lithography to a shorter wavelength, in 2012 International Symposium on Extreme Ultraviolet Lithography. 2012, Sematech: Brussels, Belgium.
6. Churilov, S.S., et al., EUV spectra of Gd and Tb ions excited in laser-produced and vacuum spark plasmas. Physica Scripta, 2009. **80**(4): p. 6.
7. Endo, A., Extendability of LPP EUV source technology in higher power (kW)/ shorter wavelength (6.x nm) operation, in EUV source workshop. 2012, http://www.euvlitho.com: Dublin, Ireland.
8. Türke, D., et al., *Concept study on an accelerator based source for 6.x nm lithography*, in *EUV source workshop*. 2012, www.euvlitho.com: Dublin, Irland.
9. *http://www.media-lario.com*.

10. Khorsand, A.R., et al., Single shot damage mechanism of Mo/Si multilayer optics under intense pulsed XUV-exposure. Opt. Express. **18**(2): p. 700-712.
11. Sobierajski, R., et al., Damage mechanisms of MoN/SiN multilayer optics for next-generation pulsed XUV light sources. Opt. Express. **19**(1): p. 193-205.
12. Spiller, E., *Reflective multilayer coatings for the far uv region.* Appl. Opt., 1976. **15**(10): p. 2333-2338.
13. Underwood, J.H. and J.T.W. Barbee, Layered synthetic microstructures as Bragg diffractors for X rays and extreme ultraviolet: theory and predicted performance. Appl. Opt., 1981. **20**(17): p. 3027-3034.
14. Vinogradov, A.V. and B.Y. Zeldovich, *X-ray and far uv multilayer mirrors: principles and possibilities.* Appl. Opt., 1977. **16**(1): p. 89-93.
15. Tsarfati, T., et al., *Nitridation and contrast of B_4C/La interfaces and multilayers.* Thin Solid Films, 2010. **518** p. 7249-7252.
16. Platonov, Y., et al., *Multilayers for next generation EUVL at 6.X nm* SPIE, 2011. **8076**(22): p. 1-9.
17. Tsarfati, T., et al., Reflective multilayer optics for 6.7 nm wavelength radiation sources and next generation lithography. Thin Solid Films, 2009. **518**(5): p. 1365-1368.
18. Andreev, S.S., et al., *Multilayered mirrors based on La/B4C(B9C) for X-ray range near anomalous dispersion of boron (lambda approximate to 6.7 nm).* Nuclear Instruments & Methods in Physics Research Section a-Accelerators Spectrometers Detectors and Associated Equipment, 2009. **603**(1-2): p. 80-82.

2 Experimental

2.1 Multilayer deposition

A deposition technique that is to be considered for multilayer deposition should provide reproducible coatings of alternating materials. For the La/B-based multilayers in this thesis the individual layer thicknesses are approximately 1.5 nm. The multilayer requires a typical period thickness reproduction accuracy within ~0.1% of its thickness. To maximize the optical contrast between the reflector and the spacer layers the interfaces should be chemically and morphologically as sharp as possible. The deposition technique that is expected to produce sharp interfaces would be the technique that allows atomic layers deposition such as the heteroepitaxial growth as is described by Wulfhekel et.al. [1]. The approach of Wulfhekel et.al. requires the accurate match of the lattice parameters of materials to minimize the stress at the interface, which limits the material choice. However, since multilayer deposition using this technique has not been developed yet for the La/B based material combination conventional deposition techniques like magnetron sputtering and e-beam evaporation were used.

The required morphological interface sharpness necessitates smoothening of the surface because of the increase in surface roughness during the typical growth process[2]. To deposit smooth layers the arriving atoms should have enough surface mobility to allow surface relaxation to prevent build up of roughening during the layer growth [3]. The lack of mobility due to low energy of the particles deposited for instance by e-beam evaporation in the case of Mo/Si multilayers grown at room temperatures introduces high interface roughness. Additional polishing of the Si layers with noble gas ions is required for high reflective coatings [4]. The advantage of this two step process is that both growth and smoothening can be optimized independently.

Smoothening by ion polishing or elevated growth temperatures, will in the case of ultrathin layers required for 6.x nm lithography probably also stimulate interface diffusion processes and/or interface compound formation. Both interface imperfections, morphological and material intermixing reduce the multilayer reflectivity similarly. Therefore the selected deposition technique should allow interface engineering to minimize the integral interface thickness. From a practical point of view the choice of the deposition technique will be determined by the same limitations required for Mo/Si multilayer mirror coating. One of which is the requirement of room temperature deposition.

The research described in this thesis was done using the Advanced Development Coater (ADC) in nanolayer Surface&Interface physics department of the DIFFER Institute. The coater was designed for the development of Mo/Si multilayers [5, 6] and has two techniques available: electron beam evaporation and magnetron sputtering. As shown in Figure 2.1, the setup is equipped with four DC magnetrons and six e-beam evaporators for layer deposition. The hot cathode Kauffman ion gun was used for nitrogen ion post treatment of deposited layers. Quartz crystal microbalances were used for layer thickness control during the e-beam evaporation. The ADC is equipped with two gas inlets per magnetron and two gas inlets via the Kauffman ion gun, allowing some flexibility during the depositions. To avoid contamination of the layers base pressure in the coater chamber was keep below 10^{-8} mbar.

The main difference between electron beam evaporation and magnetron sputtering is the energy of the emitted particles. The electron beam evaporation produces thermalized particles that have energy in the order of 0.1 eV. Magnetron sputtering on the other hand produces a more complex spectrum in both energy and species of the emitted particles. The sputtered target material is expected to have energies in the range of 1-10eV. Furthermore, the noble gas used to erode the target can bombard the mirror surface by reflection from the target or by erosion plasma extending into the area occupied by the mirror. The energy range covered can be in the range of 1-800eV, depending on the operational conditions. Because the effect of ion assistance is always present during magnetron sputtering, no additional smoothening step should be required when the magnetron working conditions are tuned correctly[7]. The operational conditions for magnetron sputtering should be optimized to provide sufficient layer smoothening and limited layer intermixing.

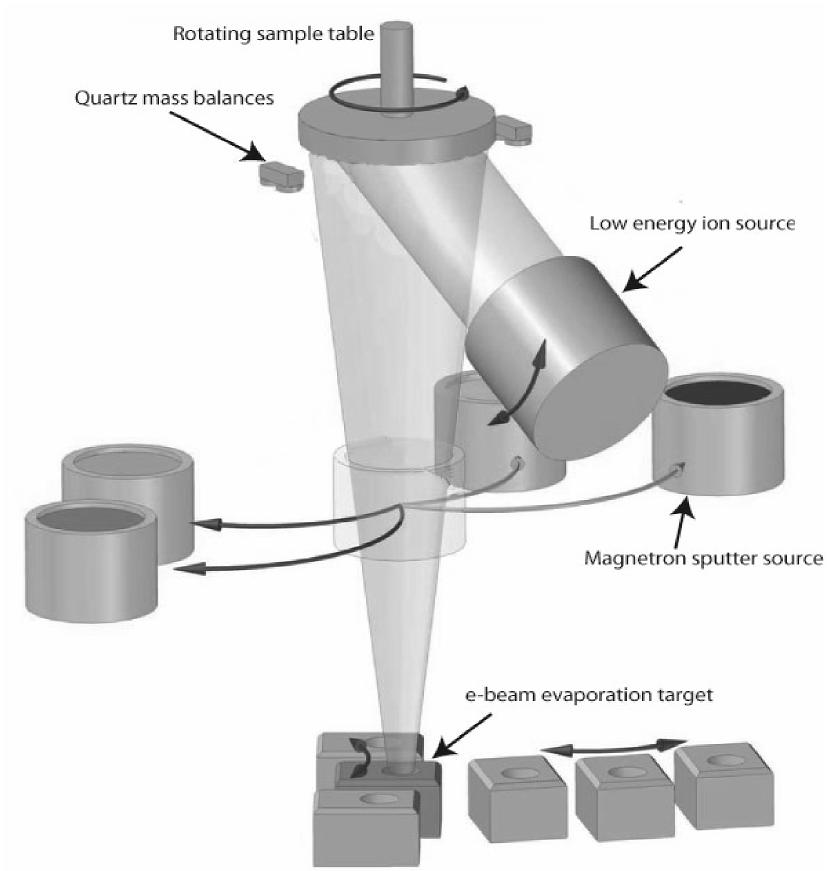

Figure 2.1 The scheme of Advanced Development Coater used for the deposition of films described in current thesis.

Most of the multilayer mirrors for reflectivity or structural characterization were deposited by a modified [6] DC magnetron sputtering technique using Ar or Kr as a sputter gas. The typical pressure during the sputtering process was in order of 10^{-4} mbar. The main difference from conventional magnetron sputtering and our setup is the distance between the magnetrons and the substrate. In our setup magnetrons are placed further from the substrate than the mostly used typical distance of 10-15 cm. In this setup the energy atoms arriving at the substrate can be reduced by increasing the pressure inside the deposition chamber. Practically magnetron deposition was preferred over e-beam evaporation because of the higher deposition rates and stability. This becomes especially beneficial for the deposition of multilayer mirrors with more than 150 periods. During magnetron deposition the layer thickness could be adjusted by calibration of the deposition rates at constant operational conditions.

In specific cases e-beam deposition was also used. In chapter 3, e-beam evaporation was used for the deposition of La/B and La/B_4C multilayer mirrors because that time magnetron sputtering of pure boron was not yet available. This part of the research focused on the comparison of the optical properties of B_4C and B based multilayers. Therefore, for consistency, it was decided to use one deposition technique for all materials. Also in chapter 5 multilayers with a low number of periods (40) were deposited using e-beam evaporation because deposition with a vapour mask was required. E-beam evaporators can be assumed as point sources. Therefore the deposition of multilayers with a gradient in the period along the radial direction over the substrate table using a vapour mask can more easily be performed than with magnetron sputtering. Finally, in chapter 6 the Cr and B_4C layers were deposited using e-beams for practical reasons and because the selection of deposition technique did not influence the main conclusion of presented research.

2.2 Characterization of multilayer mirrors

The traditional characterization of a periodic multilayer mirror designed for the extreme ultraviolet wavelength range involves two types of measurement of the reflectance. One performed with hard X-rays at grazing incidence angle (GIXR) and a second one performed "at-wavelength", so close to normal incidence in the extreme ultraviolet range (EUVR). For the current work the wavelength ranges from 6.6-7.0 nm and the measured angle is at 1.5 degree of normal incidence. The experimental geometries for EUVR and GIXR together with examples of possible curves are presented in Figure 2.1.

GIXR is sensitive to basic multilayer structure parameters. It can provide information on layer thicknesses, densities and interface roughness. However, due to uncertainties in the reconstruction of the multilayer structure from GIXR measurements, a model obtained from GIXR may not correctly describe the EUVR data. One of the origins of the mismatch between the EUVR and GIXR models is the different sensitivity to the multilayer parameters. For example, while GIXR is very sensitive to the layer thickness ratio in the multilayer period, it is less sensitive to the chemical composition of the layers. The EUVR reflectance is extremely sensitive to the layer composition, such as the presence of impurities, but data analysis is complicated by the large correlation between the model parameters.

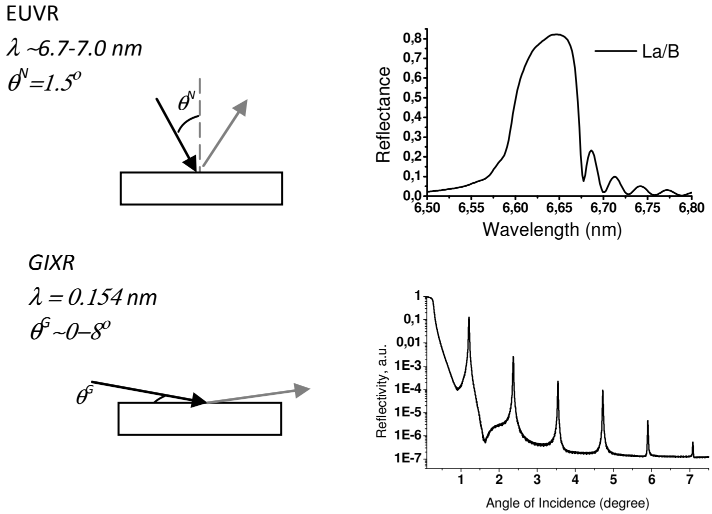

Figure 2.2 The geometry and typical data for normal incidence EUV reflectivity (EUVR) and grazing incidence X-ray reflectivity (GIXR) experiments.

Having both sets of measurements it is beneficial to perform simultaneous analysis of measured hard- and soft-X-ray data using one model (layer thicknesses, densities and materials). Simultaneous analysis would benefit from the EUVR sensitivity to the chemical composition and layer density, and from the GIXR sensitivity to layer thicknesses. The analysis can be performed by fitting of model based calculations to the measured data. The basics of the calculation of hard X-rays and EUV reflectivity from periodic multilayer structures is presented in section 2.2.1. The description of experimental data analysis is presented in section 2.2.2.

2.2.1 Calculation of GIXR and EUVR curves

The wave propagation in a homogeneous layer can be characterized using the transfer matrix[8] that connects the electric field and its first derivative at the interfaces between two layers:

$$\mathbf{M}_i = \begin{pmatrix} \cos k_{z,i} d_i & 1/k_{z,i} \sin k_{z,i} d_i \\ -k_{z,i} \sin k_{z,i} d_i & \cos k_{z,i} d_i \end{pmatrix} \tag{2.1}$$

where d_i is the layer thickness and $k_{z,i}$ is a projection of the wave vector onto the z-direction. In general $k_{z,i}$ depends on the polarization of the incident radiation:

$$k_{z,i} = \begin{cases} k_0\sqrt{n_i^2 - n_0^2\cos^2\theta} & s-polarization, \\ k_0 n_i^2 \Big/ \sqrt{n_i^2 - n_0^2\cos^2\theta} & p-polarization; \end{cases} \tag{2.2}$$

where $n_i=1-\delta_i-i\beta_i$ is the complex refractive index of a layer material, $k_0 = |\boldsymbol{k_0}| = 2\pi/\lambda$ is the absolute value of the wave vector in vacuum, λ is the incident beam wavelength and θ is the grazing incident angle[9]. The wave propagation through a system with N layers is then represented by the characteristic matrix:

$$\mathbf{M} = \mathbf{M}_N\mathbf{M}_{N-1}\ldots\mathbf{M}_2\mathbf{M}_1 = \prod_{i=N}^{1}\mathbf{M}_i \tag{2.3}$$

For periodic multilayer structures with identical periods, the multiplication of matrices M_i (2.3) can be calculated analytically [10]:

$$\tilde{\mathbf{M}}^K = \begin{pmatrix} \tilde{m}_{11} & \tilde{m}_{12} \\ \tilde{m}_{21} & \tilde{m}_{22} \end{pmatrix}^K = \begin{pmatrix} \tilde{m}_{11}U_{K-1}(a) - U_{K-2}(a) & \tilde{m}_{12}U_{K-1}(a) \\ \tilde{m}_{21}U_{K-1}(a) & \tilde{m}_{22}U_{K-1}(a) - U_{K-2}(a) \end{pmatrix} \tag{2.4}$$

Here $U_k(a) = \sin[(n+1)\arccos(a)]/\sqrt{1-a^2}$ is the Chebyshev polynomial of the second kind, $a = (\tilde{m}_{11} + \tilde{m}_{22})/2$, $\tilde{M}$ is the characteristic matrix calculated for a multilayer period and K is the number of periods in a multilayer structure. This approach is valid for unimodular matrices and can be applied to the characteristic matrices discussed here because det($\tilde{M}$) = ±1. Using Chebyshev polynomials saves computational resources in comparison with standard matrix multiplication procedures.

The reflectance amplitude is given by:

$$r = \frac{k_{z,N+1}k_{z,0}M_{12} + ik_{z,0}M_{22} - ik_{z,N+1}M_{11} + M_{21}}{k_{z,N+1}k_{z,0}M_{12} + ik_{z,0}M_{22} + ik_{z,N+1}M_{11} - M_{21}} \tag{2.5}$$

where $k_{z,0}$, $k_{z,N+1}$ are the wave vector projections in ambient and substrate media, respectively. The reflected beam intensity can be calculated by

$$I^{theory}(\theta,\lambda,\mathbf{p}) = |r|^2 I_0 \tag{2.6}$$

where $\boldsymbol{p}$ is the set of structural parameters (layer thicknesses and electron densities) and I_0 is the incident beam intensity.

2.2.2 Reconstruction of structural parameters

Theoretical curves (Eq. 2.6) for GIXR and EUVR can be determined as:

$$I = \begin{cases} I_{gixr}^{theory}(\theta,\lambda,\mathbf{p})\Big|_{\lambda=\lambda_0} & -\mathrm{GIXR} \\ I_{euvr}^{theory}(\theta,\lambda,\mathbf{p})\Big|_{\theta=\theta_0} & -\mathrm{EUVR} \end{cases} \quad (2.7)$$

According to Eq. (2.1 – 2.6) the multilayer is described by a set of individual layers with thicknesses d and a complex refractive indices *n*. An optical constants of the i^{-th} layer ($n_i=1-\delta_i-i\beta_i$) depends on its chemical composition and density:

$$\begin{aligned} \delta_i &= 2.7007\times10^{-4}\times\frac{\rho_i\lambda^2}{\mu_i}\sum_{j=1}^{\Omega_i}\omega_{ij}f_j^{(1)}(\lambda) \\ \beta_i &= 2.7007\times10^{-4}\times\frac{\rho_i\lambda^2}{\mu_i}\sum_{j=1}^{\Omega_i}\omega_{ij}f_j^{(2)}(\lambda) \end{aligned} \quad (2.8)$$

Here ρ_i is a density expressed in [g/cm^3], μ_i is the molar weight [g/mol] of a compound with Ω different atoms, ω_{ij} is atomic concentrations of atoms in a layer, f_j is the atomic scattering factor [11]. Eq. (2.8) shows that the optical characteristics of the multilayer structure are determined by its chemical composition with stoichiometry ω and density ρ.

Interface imperfections (σ_i) are taken into account by adding transition layers to the model. Parameters of interfaces are chosen according to a linear distribution of electron density between homogeneous media. Firstly, unlike the commonly used Debye-Waller or Nevot-Croce statistical factors, this approach properly considers dynamic effects. It takes into account shifts of the diffraction peaks caused by interface imperfections. Secondly, this description of the interfaces does not affect the unimodularity condition for the characteristic matrix that allows the application of equation (2.4).

To describe the period structure with a two-layer model, it is convenient to use a set of effective technical parameters:

$$\begin{cases} D = d_1 + d_2 + \sigma_1 + \sigma_2 \\ \Gamma = (2d_2 + \sigma_1 + \sigma_2)/2D \\ S = (\sigma_1 + \sigma_2)/D \\ S_\Gamma = \sigma_2/(\sigma_1 + \sigma_2) \end{cases} \quad (2.9)$$

For X-ray reflectivity the period thickness *D* influences only the diffraction peak positions. The period asymmetry *Γ* defines the intensity ratio between diffraction peaks. The part of the period that consists of interfaces layers is indicated by *S.* An asymmetry in the interface imperfections is denoted by S_Γ which determines diffraction peak amplitudes and the asymptotic behaviour of the experimental curve.

The problem of reconstruction of the structural parameters is formulated as an optimization problem for the merit functionχ^2.

$$\tilde{\mathbf{p}} = \min \chi^2(\mathbf{p}) \tag{2.10}$$

In Eq. (2.10) $\boldsymbol{p}$ is the set of technical parameters presented in Eq. (2.9). Layer densities ρ and stoichiometrical coefficients ω, $\tilde{p}$ are the resulting set of reconstructed parameters and χ^2 is a goodness of fit value similar to Pearson's criterion. For fitting the Levenberg-Marquard[12] optimization algorithm was used.

In order to reconstruct parameters from two sets of experimental data the criterion for fit quality has the form:

$$\chi^2 = \frac{1}{L_{gixr} + L_{euvr} - l}\left[\sum_{\theta} \frac{\left(I_{gixr}^{theory}(\theta, \mathbf{p})\big|_{\lambda=\lambda_0} - I_{gixr}^{\exp}(\theta)\right)^2}{\sigma_{gixr}^2(\theta)} + \sum_{\lambda} \frac{\left(I_{euvr}^{theory}(\lambda, \mathbf{p})\big|_{\lambda=\lambda_0} - I_{euvr}^{\exp}(\lambda)\right)^2}{\sigma_{euvr}^2(\lambda)}\right] \tag{2.11}$$

where L_{GIXR} and L_{EUVR} are numbers of points, σ_{GIXR} and σ_{EUV} are errors of the GIXR and EUVR curves respectively. A systematic error σ_{sys}, related to the experimental design and a random error $\sigma_{rand} = \sqrt{I}$, related to the discrete nature of the radiation are taken into account: $\sigma_{GIXR}^2(\theta) = \sqrt{\sigma_{sys}^2 + \sigma_{rand}^2}$. If errors in the experimental data are normally distributed and the number of experimental points is much larger than the number of fit parameters, the quality of the fit for a perfect model has a value of unit, $\chi^2=1$. The simultaneous fit of GIXR and EUVR is performed in chapter 5 for the analysis of La/B and LaN/B multilayer structures.

The analysis of GIXR data only is performed in chapter 6 and 7 for reconstruction of the electromagnetic field inside the structure for its further utilization in analysis of XSW data.

2.3 X-ray standing wave analysis of periodic and aperiodic thin films

The rigorous analysis of GIXR and EUVR curves is capable of providing the electron density profiles. However, due to the limited measurement range and statistical and systematic measurement errors the reconstructed profiles are not unique. The interpretation of electron density profiles is furthermore challenging because of the correlation between layer densities and compound stoichiometry. To obtain more accurate information about the atomic distribution the X-ray standing wave technique (XSW)[13] can be applied.

The XSW method is a technique based on the analysis of a secondary emission yield exited by the XSW formed in a film. XSW's are formed as the result of interference between the incident and reflected beams. In the case of analysis of non-periodic structures, the XSW can be formed at total external reflection conditions and in case of periodic multilayer structures the XSW can be formed in Bragg reflection condition. As secondary emission the X-ray fluorescence radiation or X-ray photoelectrons can be used. Unlike GIXR analysis that is sensitive to the averaged electron density profile, the XSW technique is sensitive to the atoms. The secondary emission yield exited by the XSW holds the information about the atomic profile inside the film. The detailed description of the calculation and analysis of the XSW data is presented in chapter 7.

The XSW technique can also be used to analyze the densities of thin layers. This will be shown in chapter 6. The XSW, in this case resulting from interference between incident and reflected beam at grazing incident conditions, depends on the characteristics of the reflecting layer. At low angles of incidence, a denser layer reflects more X-rays than a lower density layer. By measuring the characteristic yield as a function of angle of the incident X-rays from a thin marker layer, placed above the layer to be characterized, one can observe the intensity of the XSW field. This signal provides information about the density of the layer under investigation.

In XSW experiments, discussed in this thesis (chapters 6 and 7), the fluorescence yield measurements are used for several reasons. Firstly, the fluorescent photons have a considerably larger escape depth than photoelectrons which allows e.g. to measure the signal from all layers in a 50-period multilayer mirror (chapter 7). Secondly the measurements of the fluorescence yield do not require vacuum conditions unlike measurement of the photoelectron yield.

2.4 References

1. Wulfhekel, W., et al., *Manipulation of growth modes in heteroepitaxy: Ni/Cu(111).* Applied Physics Letters, 1996. **69**(23): p. 3492-3494.
2. Wasa, K. and S. Hayakawa, Handbook of Sputter Deposition Technology: Principles, Technology, and Applications. 1992: Noyes Publications.
3. Barabasi, A.L. and H.E. Stanley, *Fractal Concepts in Surface Growth.* 1995: Cambridge University Press.
4. Voorma, H.J., et al., *Angular and energy dependence of ion bombardment of Mo/Si multilayers.* Journal of Applied Physics, 1997. **82**(4): p. 1876-1881.
5. Louis, E., et al., Nanometer interface and materials control for multilayer EUV-optical applications. Progress in Surface Science, 2011. **86**(11): p. 255-294.
6. Yakshin, A.E., et al., Enhanced reflectance of interface engineered Mo/Si multilayers produced by thermal particle deposition. Proc. of SPIE 2007. **6517**: p. 65170I-1 - 65170I-9.
7. Eriksson, F., et al., Atomic scale interface engineering by modulated ion-assisted deposition applied to soft x-ray multilayer optics. Appl. Opt., 2008. **47**(23): p. 4196-4204.
8. Born, M. and E. Wolf, *Principles of Optics.* Seventh ed. 2000, Cambridge: Campridge university press.
9. Attwood, D., Soft X-Rays and Extreme Ultraviolet Radiation: Principles and Applications. 2007: Cambridge University Press.
10. Born, M. and E. Wolf, *Principles of optics.* 1999: Cambridge University Press.
11. http://www-cxro.lbl.gov, *CXRO X-ray database.*
12. Press, W.H., Numerical Recipes 3rd Edition: The Art of Scientific Computing. 2007: Cambridge University Press.
13. Zegenhagen, J. and A. Kazimirov, *The X-ray Standing Wave Technique: Principles and Applications*: World Scientific Publishing Company Incorporated.

3 Spectral properties of La/B - based multilayer mirrors near the boron K absorption edge

The spectral properties of La/B, La/B_4C, and LaN/B, LaN/B_4C multilayer mirrors have been investigated in the 6.5-6.9 nm wavelength range based on measured B and B_4C optical constants. Experimentally it is verified to what extent measured and tabulated optical constants are applicable for simulations of the reflectivity of these short period multilayer mirrors. The measured maximum reflectance at various wavelength values around the boron-K absorption edge is compared to calculated values from model systems. The measured reflectance profiles of La/B and La/B_4C show a maximum at a slightly larger wavelength than calculations would predict based on the measured B and B_4C optical constants. This is explained by the influence of a formed boron-lanthanum compound on the wavelength where the multilayer shows maximum reflectance. The maximum reflectance profiles of LaN/B and LaN/B_4C multilayers can be described accurately by using the same boron atomic scattering factors, indicating boron in the LaN/B_4C multilayer to be in a similar chemical state as boron in the LaN/B multilayer. It also indicates that nitridation of the La layer in the multilayer prevents the formation of La-B compounds. We show that the optimal wavelength for boron based optics is about 6.65 nm and depends on the B chemical state. Finally, using the measured B optical constants we are able to calculate the spectral response of the multilayers, enabling the prediction of the optimal parameters for the above mentioned multilayers.

3.1 Introduction

Optics for extreme ultraviolet radiation of 6.5-6.9 nm wavelength is interesting for many applications. For example a new generation photolithography or free electron lasers requires optics that reflects at these wavelengths.

It is shown [1-5] that around 6.6 nm wavelength the highest normal incidence reflectance is obtained with multilayer mirrors based on lanthanum as reflector and boron as spacer material. Boron is the appropriate spacer material because of the close proximity to the boron K-absorption edge. In previous work La/B_4C multilayers have been studied [6-8], replacing boron with B_4C to simplify the deposition process. Measured EUV reflectance from real La/B_4C multilayers is significantly lower than the value predicted theoretically for ideal structures. One of the factors limiting the EUV reflectance is intermixing at the interfaces between La and B. It has been shown [9] that nitridation of the La layer can reduce intermixing by formation of the chemically stable LaN compound.

A wavelength dependent reflectivity study of multilayers is interesting from both applied and fundamental point of view, particularly since key in designing the next generation EUVL optics will be the matching of its optimum wavelength to that of the candidate EUV sources based on Tb or Gd. The published emission spectra from these materials show the highest intensities at 6.52 and 6.78 nm respectively [10]. To find optimal matching of optics and sources, knowledge of wavelength dependent reflectance is required. On the other hand, multilayer reflectivity spectra recorded in the vicinity of the B absorption edge hold information about the B chemical state inside the multilayer [11-13].

Here we have studied spectral properties of La-/B- based multilayers with four different layer compositions: La/B, La/B_4C, LaN/B and LaN/B_4C. We propose a way to predict the behaviour of model structures for these multilayers. Two major factors determine the multilayer reflectivity profile: the optical constants of the materials in the multilayers and the structure of the multilayers. In this paper we mainly examine the influence of the B optical constants on the La-/B- based multilayer reflectivity profile. The theoretical description of the wavelength dependency of the multilayer reflectivity matches the measured values for all material combinations best when using the measured boron optical constants, thus enabling the prediction of the optimal multilayers parameters and the theoretical maximum reflectivity for La/B, La/B_4C, LaN/B and LaN/B_4C multilayer mirrors.

3.2 Application of measured optical constants for simulation of multilayer reflectivity

In resonant Bragg conditions the multilayer mirror peak reflectance can be calculated analytically [2, 14]. We consider mirrors with sufficient film thickness to show no influence of the substrate material on the reflectance. The multilayer peak reflectance mainly depends on the optical contrast between reflector and spacer. Boron has been chosen as a spacer because of its extremely low absorption in the vicinity of its absorption edge at 188 eV (or 6.6 nm). Lanthanum is chosen as reflector for its optical contrast with B and low absorption at this wavelength range. A maximum amount of bi-layers is now contributing to the constructive interference that forms the peak reflectance.

The most complete database of optical constants in the soft and hard X-ray wavelength range has been published by Henke et.al. [17] and can be obtained from the Centre for X-Ray Optics (CXRO) web site [18]. Henke optical constants work perfectly for wavelengths far from the absorption edges. Therefore, the CXRO database can be used for La, but for boron in the 6.x nm wavelength range the optical constants can be less accurate since there are only two values of boron atomic scattering factors measured near 6.6 nm, namely at 6.44 and 6.76 nm. All other plotted values have been calculated [17]. Possible shifts of the boron absorption edge due to chemical interaction to foreign species, for example carbon, cannot be taken into account in calculations. Furthermore the used layer thickness of 1.5 nm is of the same order as the thickness of the interfaces (approximately 1 nm), indicating that in case of interface compound formation (here most likely LaB_6) it will occupy most of the spacer layer volume and will thus affect the optical constants. For example Ksenzev, using a photon-in-photon-out technique [12], found that the difference of the B adsorption edge in Ru/B_4C and W/B_4C multilayers is 1 eV [19].

In this work we have used measured B [15] and B_4C [16] optical constants. Pure boron optical constants have been calculated through transmission measurements of thick e-beam deposited B films (29, 58 and 93 nm) deposited onto a C coated grid. The optical constants of magnetron deposited B_4C films have been similarly calculated from the transmission measurements on films with thicknesses of 54, 79 and 112 nm. In both cases, the use of three different thicknesses enabled excluding effects of surface oxidation [15] [16].

The optical constants of mixed materials, based on compound composition and density, and knowing the real (f_1) and imaginary (f_2) part of the atomic scattering factors of the materials, can be calculated according to Eq. 3.1.

To extract the B scattering factors in the B_4C compound of the measured B_4C films [16], carbon and oxygen have to be taken into account since they account for a significant amount of the sample volume. This model of B atomic scattering factors is labelled as B-compound model. Models with B atomic scattering factors reconstructed form the measured B film are labelled B-atomic model. The CXRO database is used for the scattering factors of elemental materials with absorption edges far from our wavelength range (6.5-6.9 nm). The presence of C and O by itself has almost no influence on the wavelength dependent boron optical constants in a B_4C compound, except that the presence of O and C increases the absorption of the spacer layer (A possible shift of B optical constants due to boron oxide or boron carbide formation is not considered here yet). Figure 3.1 shows the calculated B atomic scattering factors f_2 from the boron and B_4C film together with data from the CXRO database. There is a noticeable difference in the absorption onset: in the B_4C film the B absorption edge is shifted 0.02 nm (or 0.6 eV) to a shorter wavelength with respect to the B film. This shift is the result of the B electron binding energy chemical shift that is a consequence of the boron carbide formation. The error bars in Figure 3.1 indicate the uncertainty in the determination of the film density. The wavelength accuracy is determined by the photon energy accuracy which is 0.007% [16] or 0.4 pm for 6 nm radiation.

$$\begin{gathered} n = 1 - \delta + i\beta \\ \delta = \frac{r_0 \lambda^2}{2\pi} \frac{\rho N_A}{MW} \sum_i n^i f_1^i \\ \beta = \frac{r_0 \lambda^2}{2\pi} \frac{\rho N_A}{MW} \sum_i n^i f_2^i \end{gathered} \tag{3.1}$$

To illustrate the influence of different chemical states of B on the multilayer reflectivity, La/B_4C peak reflectance spectra have been calculated for multilayer structures without roughness or intermixing and are shown in Figure 3.2. The two different data sets are used to reconstruct the B_4C optical constants. First, the Soufli et al. [16] measured B_4C optical constants (indicated as B-compound), and second, a mix model of 4B+1C (indicated as B-atomic) with the optical constants calculated [20] according to Eq. 3.1, using data of a B film measured by Fernandez et al [15]. Finally, the optical constants for 4B+1C are calculated with B and C atomic scattering factors obtained from the CXRO database [17] (B_4C (CXRO)).

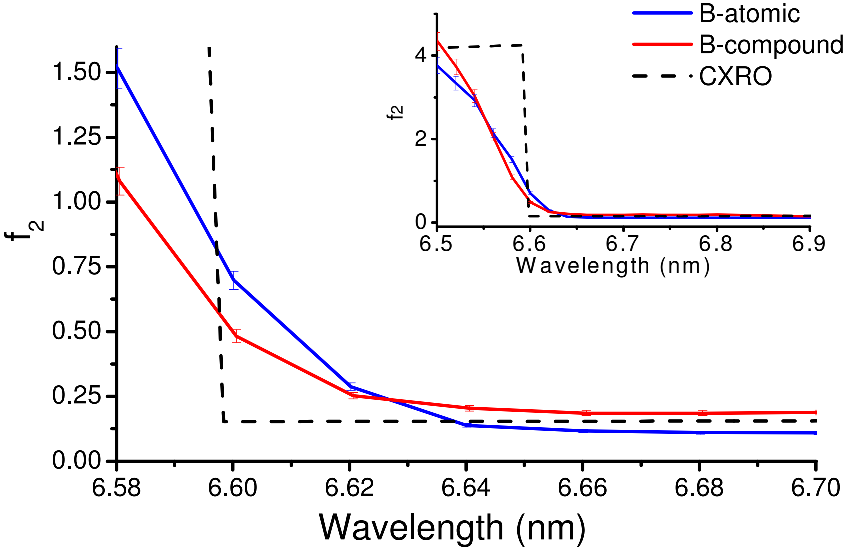

Figure 3.1 Boron atomic scattering factors obtained from a B film (B-atomic) [15], a B_4C film (B-compound) [16] and the CXRO database [17].

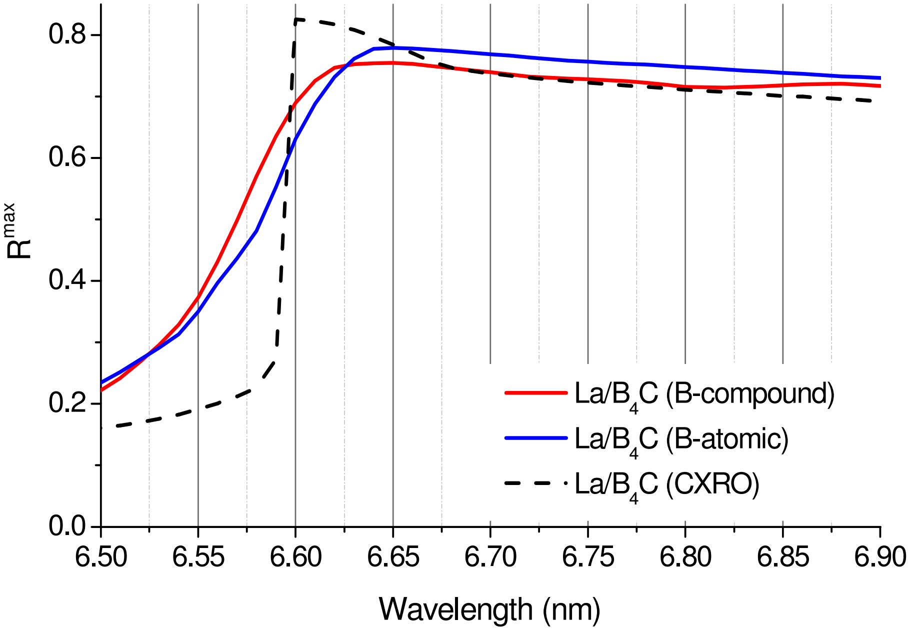

Figure 3.2: Analytical calculation of a perfect La/B4C multilayer for different B4C optical constants, namely – measured B_4C optical constants (B-compound)[16], measured B atomic scattering factors used to calculate B_4C optical constants (B-atomic) [15] and values calculated from elemental data from ref. [17].

Similar to Figure 3.1 it is observed that the wavelength of maximum reflectance is 0.02 nm longer for B_4C (B-atomic) than for B_4C (B-compound). Both reflectivity spectra calculated from measured optical constants are shifted to longer wavelength with respect to calculations based on CXRO data. The most striking difference between database and the measured optical constants in Figures 3.1 and 3.2 is observed around the absorption edge. Where the CXRO data shows a steep drop in reflectance for a wavelength below the edge, the measured data result in a more gradual drop in reflectance.

For longer wavelength, further from the absorption edge, the value of the multilayer reflectance calculated using the B-atomic model is slightly higher than when the B-compound model is used. The boron chemical state cannot influence the absolute level of reflectance far from the absorption edge. The difference can be explained assuming an error in the film density, or the determination of the B_4C or B film composition.

To assess the validity of the measured optical constants for our multilayers, we have performed a set of reflectivity spectral measurements of La-/B- based multilayers at different angles of incidence that allows us to study multilayer reflectivity at different wavelength, a method described by Spiller [11]. These measurements are described in section 3.4 of this chapter.

3.3 Experimental

La/B, La/B_4C and LaN/B, LaN/B_4C multilayers consisting of 50 bi-layers, with a bi-layer thickness of approximately 4 nm have been made in an UHV environment of $1*10^{-8}$ mbar [21]. La, B and B_4C layers were deposited at room temperature using electron beam evaporation. LaN was prepared by low energy N-ion post treatment of each La layer. Layer thicknesses were controlled by quartz crystal oscillator microbalances. Natively oxidized super polished Si wafers have been used as substrate.

For comparison with the measured data, the simulations of the reflectance of the different multilayer compositions described in the next chapter require individual models. Initially the models contain 50 equal bi-layer periods with layer thickness based on the quartz crystal oscillator microbalance values obtained during coating. Furthermore, the bulk values of material density are used. To improve these initial models each deposited multilayer was characterized using grazing incidence hard x-ray (Cu-K_α) angular dependent reflectance measurements (GI-XRR). Calculated GI-XRR spectra were fit to the measured spectra using IMD [22] and similar homemade software. In the modelling the optical constants are calculated using the Mat Lab toolbox [20] and interface roughness is taken into account by applying the Debby-Waller factor. Layer thickness, density and interface roughness were the free parameters during fitting. The reflectance around 6.6 nm has been measured at the beam line of the Physikalisch Technische Bundesanstalt (PTB, Berlin) at the BESSY II synchrotron radiation source using sigma-polarized soft X-ray radiation. The measurement setup has a relative uncertainty of the intensity measurements equal to 0.14%. The wavelength determination is accurate within 0.014% or 0.9 pm for 6.6 nm [23].

GI-XRR and soft X-rays normal incidence reflection are sensitive to different multilayer parameters. GI-XRR is more sensitive to layer roughness and individual layer thickness, while soft X-ray reflection is more sensitive to layer density and layer composition. Hard X-ray reflectivity data alone has not been sufficient to provide a model that would fit the measured soft X-ray reflection, not even far from the absorption edge, where there is no significant influence of the B chemical state. Models for simulation of the soft X-ray reflectivity at different angles of incidence have been fitted to soft X-ray reflection spectra recorded at 1.5° of normal incidence. The models obtained from GI-XRR data fitting served as starting points for soft X-ray reflectance data fitting.

Unlike calculations presented in the first section of this chapter, where simplified analytical dependencies are used, the experimental data have been simulated using the Fresnel matrix formalism optimized for periodic bi-layer structures [24].

3.4 Measurements and analysis

For all four multilayers described in the previous section, wavelength depended reflectance spectra have been measured at various angles of incidence. In order to reduce the large amount of soft X-ray reflectance data, the maximum reflectance and the corresponding wavelength at which this reflectance occurs were determined for each wavelength scan. Furthermore, each wavelength of maximum reflectance has been simulated using the model described above. Figure 3.3 presents a comparison of measured and simulated results normalized to the highest reflectance in the wavelength plot.

Figure 3.3(a) shows that the simulated La/B reflectivity profile shows a maximum at a wavelength that is 0.02 nm lower than experimentally observed. Figure 3.3(b) however shows that there is no significant shift between the measured and calculated reflectivity profiles of LaN/B multilayer. The observed

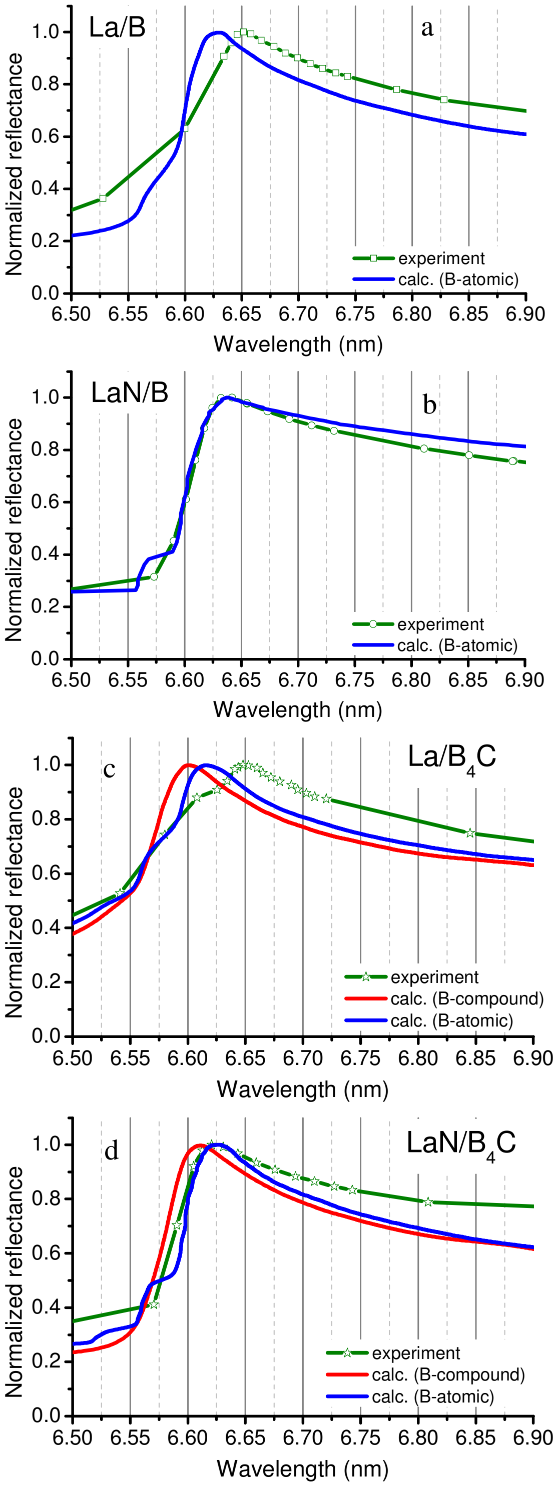

shift in the La/B case can only be explained by a change in the boron optical constants induced by a chemical shift of the B-K electron binding energy, most likely due to La-B compound formation, probably LaB_6. The similar shape and position of the calculated and measured reflectivity profiles of LaN/B multilayers indicate that in this material combination the B atoms remain in the atomic state, proving that nitridation of the La layers reduces the intermixing of lanthanum and boron. Furthermore, for the wavelength range shorter than where the maximum reflectance occurs, a clear mismatch of experimental and calculated data is observed for La/B (Figure 3.3(a)): around 6.60 nm the curves cross, hinting that part of the boron might still be in an elemental state.

Figure 3.3: Normalized maximum reflectance of measured samples and calculations using measured boron and B_4C optical constants.

For the LaN/B combination (Figure 3.3(b)) at longer wavelength, a different slope is observed. This is a consequence of a deviation of the model and the real multilayer structure. Probably in this case the accuracy of determination of the lanthanum content per bi-layer and the thickness of the intermixed zone at the interfaces is not sufficient to reconstruct the shape of the reflectivity profile. This type of model variations can slightly change the slope of the reflectance profile, but cannot change the position of the reflectance maximum more than 0.005 nm.

A more complicated picture is observed in the La/B_4C reflectivity profile. Figure 3.3(c) shows the presence of at least two distinct wavelengths pointing to absorption edge phenomena. The maximum reflectance of the experimental data in Figure 3.3(c) is at the same position as in La/B profile of Figure 3.3(a), indicating similar La-B compound formation resulting in a B absorption edge around 6.65 nm. The shape of the measured reflectivity profile in the wavelength range below the reflectance maximum can be explained by the presence of the B atoms in a different chemical state, resulting in absorption edge phenomena at a shorter wavelength than 6.65 nm. Calculations have been performed with two sets of optical constants: B_4C-(B-atomic) and B_4C-(B-compound). Comparing experimental values to both calculations, the second absorption edge in the experiment is closer to the B_4C-(B-atomic) model than to the B_4C-(B-compound), although a mix of more than two species cannot be excluded. Therefore we suggest that at least part of the boron is in the elemental state. Figure 3.3(d) shows the results of the LaN/B_4C multilayer together with the B_4C-atomic and compound models. Remarkably the profile of the experiment curve matches nicely with the B_4C-(B-atomic) model but less accurate to the B_4C-(B-compound) model. Since the LaN used in Figure 3.3(b) is the same as in Figure 3.3(d), it is assumed that nitridation reduces the intermixing at the interfaces significantly in both cases. This would imply that the boron in the B_4C layers has a similar optical response as the measured boron film, probably because it is in an elemental state. This would imply that the B_4C layer is more a mix of B and C, rather than the B_4C compound. Figure 3.3 shows that the optical response of lanthanum-boron based multilayers is complex and cannot be predicted accurately enough from database values. The exact composition and chemical interaction of these nanometer thin layers determines the optical response near the absorption edge and therefore the optimum performance in any application.

3.5 Theoretical optimization

Different applications can pose different requirements on the optics. For example, the use of multilayer mirrors as monochromator for soft X-ray radiation requires high peak reflectivity in combination with a small bandwidth, while projection photolithography requires high integrated reflectance from the stack of several mirrors over a certain bandwidth.

In this section we present a theoretical optimization of the four material combinations, La/B, La/B_4C and LaN/B, LaN/B_4C, in terms of the maximum achievable reflectance and the corresponding wavelength for an angle of incidence of 1.5^o with respect to the surface normal.

Although we were not able to perfectly fit the measured reflectivity profiles with B and B_4C optical constants measured from thick films, the match is good enough to use them to investigate the multilayer composition that would perform best in the vicinity of the B absorption edge. In the previous section the best fit of the measured reflectivity profiles is obtained using B atomic scattering factors calculated from a measured boron film. These scattering factors are used here for B and for B_4C in modelling of multilayers.

In general the bi-layer thickness (Λ) determines the wavelength of maximum reflectance. However, the reflector to bi-layer thickness ratio Γ can affect both the maximum reflectivity as well as the width of the reflectance peak, represented by the full width at half the maximum value (FWHM). In this section we optimized the Γ ratio as well as the number of bi-layers required to have the highest reflectance values. This is a different situation than in the previous section where we modelled the actually deposited multilayers. Therefore, the wavelength of maximum reflectance for the optimized multilayers in this section can deviate from the data presented in Figure 3.3.

The results of optimization for different multilayer compositions are presented in table 3.1. As in the previous section, calculations use the Fresnel matrix formalism optimized for ideal periodic bi-layer structures [24].

ML composition	Γ, d_{La}/Λ	Λ, nm	Optimal wavelength, nm	Period number	R^{max}, %	FWHM @ optimal wavelength, nm
La/B	0.39	3.34	6.66	175	80.5	0.070
LaN/B				160	80	0.076
La/B_4C	0.41		6.65	185	77.5	0.060
LaN/B_4C				170	77.5	0.066

Table 3.1 calculated parameters of the optimized multilayers.

The table 3.1 shows that optimum Γ for B_4C based multilayers is slightly higher than for B-based multilayer, which is attributed to the larger absorption in B_4C. The presence of nitrogen in the La layers has almost no influence on the multilayer spectral properties and optimal parameters except for the amount of periods. To obtain optimized reflectance in LaN/B based multilayer requires 15 periods less than for La/B, which is the result of the slightly more favourable optical constants of LaN. The reduced optimal number of periods for LaN explains the slight increase in FWHM of these multilayers.

Table 3.1 also shows that B-based multilayers have a higher maximum reflectance than B_4C-based multilayers. The reason for this is that C in B_4C results in a high absorption of the spacer layer. Since the same scatter factors are used to calculate the boron or B_4C layers no significant difference in critical wavelength is observed. The minor shift of the optimal wavelength of B_4C based multilayers with respect to B-based multilayers can be explained by the change in optical contrast in the multilayers due to presence of C, resulting in a different optimum Γ.

The presented calculations for optimized reflectance can serve as a starting point to obtain maximum reflectance experimentally. However, in this section we ignored the influence of interface imperfections on the multilayer reflectivity profile, as well as possible compound formation. As we experimentally showed in the previous section, compound formation can explain the shift of the optimal wavelength.

3.6 Discussion

In the section 3.2, analytical formulas have been used where in the optimization section of this chapter the matrix formalism has been applied. Both approaches are able to calculate reflectance spectra as well as peak reflectance and FWHM. When only optimization of peak reflectance is required, it is much faster to use the analytical approach, but for determining the exact shape of the peak it lacks accuracy and the matrix formalism or recursive Parratt equations [25] should be employed.

In photolithography, optimizing the multilayer mirror performance is required to match the reflectivity spectra with the source emission and photo resist absorption spectra. Reversely, the performance of possible mirrors is input in selecting the source. The convolution of source spectrum and mirror reflectance determines the best combination.

Calculated ideal reflectivity spectra show that the optimal source wavelength should be around 6.66 nm. For a wavelength larger than 6.66 nm there is only a weak dependency on the wavelength, whereas for smaller wavelength, crossing the boron edge, the reflectance drops dramatically. For example decreasing the wavelength to 6.60 nm will reduce the reflectance to 40% of the optimal reflectivity. In the experimental section of this chapter, from multilayer reflectivity profiles it is observed that a pronounced maximum between 6.62 and 6.66 nm exists, where the exact optimal wavelength depends on the B compound.

As discussed in section 3.4, the optical properties in the vicinity of the B-absorption edge of our thin B_4C layers in the multilayer stack show clear similarities with B in a thick film, rather than with the optical properties of a B_4C film, which could be an indication that part of the B is in its elemental state. This can be understood since boron carbide with the B_4C stoichiometry is a complex material consisting of $B_{11}C$ icosahedra and C-B-C chains [26]. Most likely the B_4C layer thickness (~2 nm) in the multilayer is not enough to form this complex B_4C structure. The detailed study of the chemical interactions in La-B_4C systems, including the influence of nitridation, will be topic of future studies.

The observed dependency of the critical wavelength on the B chemical compound can be associated with a shift of the B-1s electron binding energy. Our X-ray photoelectron spectroscopy analysis has shown that this electron binding energy in a lanthanum-boride shifts to lower energy with respect to bulk B and to higher energy when B resides in a thick film of boron-carbide. The influence of chemical bonds on the B-1s electron binding energy opens possibilities to shift the optimal wavelength to smaller values by replacing B with a compound with a larger B-1s electron binding energy, which is the case in for example BN.

3.7 Conclusions

It has been shown that for simulations of the multilayer reflectivity of La/B, La/B_4C, LaN/B and LaN/B_4C systems near the boron absorption edge, the boron chemical state has to be taken into account. From experimental data of La/B and La/B_4C multilayers it is observed that a significant amount of boron is probably bound to La. This results in a shift of the B absorption edge to a longer wavelength, which significantly changes the optical properties. The reflectivity of LaN/B and LaN/B_4C multilayers can be well described by using the measured atomic B optical constants, which suggests that in both multilayers boron atoms are in a similar state as in a boron film. In our case, for the calculation of the reflectance of short period La/B_4C and LaN/B_4C multilayers, it is best to use the

B scattering factors to simulate B_4C optical constants instead of using measured B_4C optical constants.

Numerical analysis has shown that maximum reflectance can be obtained for B-based multilayers near $\lambda = 6.66$ nm. However, the influence of the actual multilayer structure, like interface imperfections and ultra-thin film chemical composition, may shift the optimal wavelength in both directions.

3.8 References

1. A. M. Hawryluk and N. M. Ceglio, “Wavelength considerations in soft-x-ray projection lithography,” Appl. Opt. **32**, 7062-7067 (1993).
2. A. V Vinogradov., I. A. Brytov, A. Ya. Grudskii., M. X. Kogan, and I. V. Kozhevnikov, *Zerkal'naya rentgenovskaya optika* (X-ray Mirror Optics, Leningrad: Mashinostroenie, 1989).
3. E. Spiller, *Soft X-ray Optics* (SPIE optical Engineering press, 1994).
4. T. Tsarfati, R. W. E. van de Kruijs, E. Zoethout, E. Louis, and F. Bijkerk, “Reflective multilayer optics for 6.7 nm wavelength radiation sources and next generation lithography,” Thin Solid Films **518**, 1365-1368 (2009).
5. C. Montcalm, P. A. Kearney, J. M. Slaughter, B. T. Sullivan, M. Chaker, H. Pépin, and C. M. Falco, “Survey of Ti-, B-, and Y-based soft x-ray-extreme ultraviolet multilayer mirrors for the 2- to 12-nm wavelength region,” Appl. Opt. **35**, 5134-5147 (1996).
6. J. M. Andre, P. Jonnard, C. Michaelsen, J. Wiesmann, F. Bridou, M. F. Ravet, A. Jerome, F. Delmotte, and E. O. Filatova, “La/B4C small period multilayer interferential mirror for the analysis of boron,” X-Ray Spectrom. **34**, 203-206 (2005).
7. S. Andreev, M. Barysheva, N. Chkhalo, S. Gusev, A. Pestov, V. Polkovnikov, D. Rogachev, N. Salashchenko, Y. Vainer, and S. Zuev, “Multilayer x-ray mirrors based on La/B4C and La/B9C,” Tech. Phys+. **55**, 1168-1174 (2010).
8. S. S. Andreev, M. M. Barysheva, N. I. Chkhalo, S. A. Gusev, A. E. Pestov, V. N. Polkovnikov, N. N. Salashchenko, L. A. Shmaenok, Y. A. Vainer, and S. Y. Zuev, “Multilayered mirrors based on La/B4C(B9C) for x-ray range near anomalous dispersion of boron (lambda approximate to 6.7 nm),” Nuclear Instruments & Methods in Physics Research Section a-Accelerators Spectrometers Detectors and Associated Equipment **603**, 80-82 (2009).
9. T. Tsarfati, E. Zoethout, R. W. E. van de Kruijs, and F. Bijkerk, “Nitridation and contrast of B4C/La interfaces and multilayers,” Thin Solid Films **518** 7249-7252 (2010).
10. S. S. Churilov, R. R. Kildiyarova, A. N. Ryabtsev, and S. V. Sadovsky, “EUV spectra of Gd and Tb ions excited in laser-produced and vacuum spark plasmas,” Phys. Scr. **80**, 6 (2009).
11. E. Spiller, *“Refractive index of amorphous carbon near its K-edge”* Appl. Opt. **29,** 19-23 (1990).
12. D. Ksenzov, T. Panzner, C. Schlemper, C. Morawe, and U. Pietsch, “Optical properties of boron carbide near the boron K edge evaluated by soft-x-ray reflectometry from a Ru/B4C multilayer,” Appl. Opt. **48**, 6684-6691 (2009).

13. D. Ksenzov, C. Schlemper, and U. Pietsch, “Resonant soft x-ray reflectivity of Me/B4C multilayers near the boron K edge,” Appl. Opt. **49**, 4767-4773 (2010).
14. A. V. Vinogradov and B. Y. Zeldovich, “X-ray and far uv multilayer mirrors: principles and possibilities," Appl. Opt. **16**, 89-93 (1977).
15. M. Fernández-Perea, J. I. Larruquert, J. A. Aznárez, J. A. Méndez, M. Vidal-Dasilva, E. Gullikson, A. Aquila, R. Soufli, and J. L. G. Fierro, "Optical constants of electron-beam evaporated boron films in the 6.8-900 eV photon energy range," J. Opt. Soc. Am. A **24**, 3800-3807 (2007).
16. R. Soufli, A. L. Aquila, F. Salmassi, M. Fernández-Perea, and E. M. Gullikson, "Optical constants of magnetron-sputtered boron carbide thin films from photoabsorption data in the range 30 to 770 eV,” Appl. Opt. **47**, 4633-4639 (2008).
17. B. L. Henke, E. M. Gullikson, and J. C. Davis, “X-Ray interactions: photoabsorption, scattering, transmission, and reflection at E = 50-30,000 eV, Z = 1-92,” Atomic Data and Nuclear Data Tables **54**, 181-342 (1993).
18. E. Gullikson, web site The Center for X-Ray Optics (1995-2010), retrieved http://henke.lbl.gov/optical_constants/.
19. D. Ksenzov, “Interaction of femtosecond x-ray pulses with periodical multilayer structures,” (PhD Thesis, Siegen University, Siegen, 2010).
20. Z. Jiang, Toolbox: X-ray Refraction of Matter, MatLab Central, (2004).
21. E. Louis, A. E. Yakshin, T. Tsarfati, and F. Bijkerk, “Nanometer interface and materials control for multilayer EUV-optical applications,” Progress in Surface Science **86**, 255-294 (2011).
22. D. L. Windt, “IMD - Software for modeling the optical properties of multilayer films,” Comput. Phys. **12**, 360-370 (1998).
23. F. Scholze, C. Laubis, C. Buchholz, A. Fischer, S. Plöger, F. Scholz, H. Wagner, G. Ulm, “Status of EUV reflectometry at PTB,” SPIE **5751** 749–758 (2005).
24. M. Born and E. Wolf, *Principles of Optics, Seventh ed.* (Campridge university press, Cambridge, 2000).
25. L. G. Parratt, “Surface studies of solids by total reflection of x-rays,” Phys. Rev. **95**, 359-369 (1954).
26. G. H. Kwei and B. Morosin, “Structures of the boron-rich boron carbides from neutron powder diffraction: implications for the nature of the inter-icosahedral chains,” J. of Phys. Chem. **100**, 8031-8039 (1996).

4 Wavelength selection for multilayer coatings for the lithography generation beyond EUV

The spectral properties of LaN/B and LaN/B_4C multilayer mirrors have been investigated in the 6.5-6.9 nm wavelength range, based on measured B and B_4C optical constants. We show that the wavelength of optimal reflectance for boron based optics is between 6.63 and 6.65 nm, depending on the boron chemical state. The wavelength of the maximum reflectance of the LaN/B_4C multilayer system is confirmed experimentally. Calculations of the wavelength-integrated reflectance for perfect 10-multilayer-mirror stacks show that a B-based optical column can be optimized for a wavelength larger than 6.65 nm.

4.1 Introduction

Reducing the operating wavelength in advanced photolithography while maintaining the lithography machine's productivity is a traditional way to enable improved imaging for the last 20 years. The transition from 13.5 nm to 6.5-6.9 nm optical lithography offers a possibility to combine high imaging capabilities using a manageable process window (1). It is shown (2-7) that around 6.6 nm wavelength the highest reflectance is obtained with multilayer mirrors based on lanthanum as a reflector and boron as a spacer material. Boron is the preferred spacer material for this wavelength because of the close proximity to the boron K-absorption edge (8, 9).

The mirrors for this next generation photolithography require twice shorter bi-layer thickness and approximately 4 times more layers than Mo/Si mirrors for 13.5 nm EUVL. The need for a larger amount of periods significantly reduces the optical bandwidth of the multilayer and thus of a ten-mirror La/B_4C based optics: 0.6 % compared to 2 % for Mo/Si. To enhance the reflectivity of La/B-based multilayers, it might be beneficial to use the technology of contrast enhancement of the interface diffusion barriers similar to that applied in existing 13.5 nm deposition technologies (10). Currently the measured normal incidence reflectance from real La/B-based multilayers is significantly lower than the theoretically predicted value. One of the factors limiting the reflectance is intermixing at the interfaces between La and B. It has been shown (11) that nitridation of the La layer has a high potential to reduce intermixing due to the formation of the chemically more stable LaN compound.

Key in design of the next generation EUVL optics will be to match its optimum wavelength to that of the candidate EUV sources based on, for instance, Tb or Gd plasmas. The published emission spectra (12) from these materials show the highest intensities at 6.52 and 6.78 nm respectively.

Here we have studied the spectral properties of LaN/B and LaN/B_4C multilayer mirrors by examining the influence of the B and B_4C optical constants on the B-based multilayer reflectivity profile. We confirm the theoretically obtained wavelength dependence of LaN/B_4C mirrors with experimental data and find clear data on EUV-optical properties of candidate materials and optics.

4.2 Application of measured optical constants for simulation of multilayer reflectivity

Calculations of multilayer reflectivity profiles strongly depend on the used optical constants. The most complete optical constants database in the soft and hard X-ray wavelength range has been published by Henke et. al. (15) and its most updated version can be obtained from the Centre for X-Ray Optics (CXRO) web site (16).

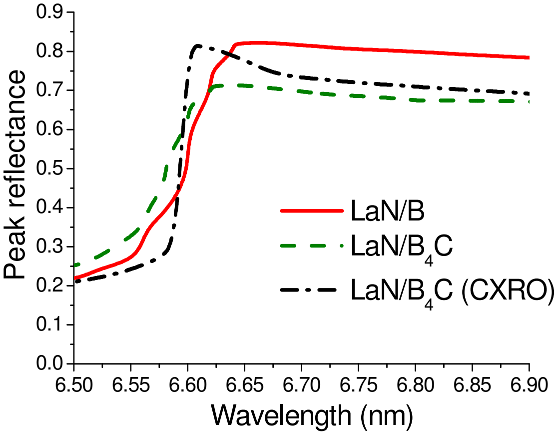

Figure 4.1 Peak reflectivity of an perfect LaN/B multilayer mirror calculated using measured B optical constants (13) (line) and a LaN/B$_4$C multilayer mirror calculated using measured (14) (dashed) and Henke (15) (dashed-dotted) optical constants.

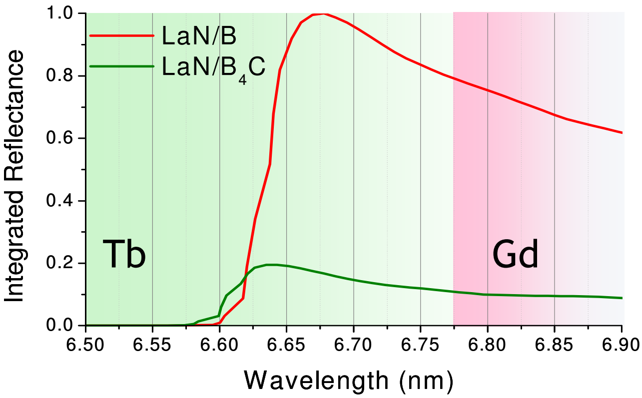

Figure 4.2 Normalised integrated reflectivity for a 10-element mirror system consisting of LaN/B (red) and LaN/B$_4$C (green) multilayer mirrors, as calculated using measured optical constants for B (13) and B$_4$C (14). The region of the Tb radiation spectrum is indicated with a green background and of Gd with a red background (12).

The CXRO optical constants for La have been recently updated with experimental values (17). For boron in the 6.x nm wavelength range the CXRO optical constants are based on theoretical calculations using the independent atom approximation and can be less accurate especially in the vicinity of the absorption edge. In addition, possible shifts of the boron absorption edge due to chemical interaction with other species, for example carbon, should be taken into account. The solution to this problem is to use measured B (13) and B_4C (14, 18) optical constants.

The wavelength dependencies of the peak intensities calculated for LaN/B and LaN/B_4C multilayer mirrors using measured B and B_4C and CXRO B_4C optical constants are shown in Figure 4.1. Here calculations were done for ideal multilayer model as described in details here (19). A significant difference between the CXRO database and measured optical constants is observed around the adsorption edge: the CXRO data shows a steep drop in reflectance for a wavelength below the edge, whereas the use of the measured data results in a more gradual drop in reflectance. Comparing reflectivity profiles of B- and B_4C-based multilayers calculated with measured optical constants, we observe a minor shift of the wavelength of maximum reflectance. For LaN/B_4C the maximum reflectivity can be achieved at λ=6.63 nm while for LaN/B this maximum reflectance is found at λ=6.65 nm. This difference can be explained by the 1s B binding energy chemical shift caused by formation of the boron rich carbide. The most common structure of B_4C contains four $B_{11}C$ icosahedrons and CBC chain as a unit cell (20-22), while pure crystalline or amorphous boron contains B_{12} icosahedrons (23). Because of the large variety of possible bonds in B_4C(20) we cannot speak about a well defined absorption edge position. The total effect of the presence of 20% of C in the boron matrix shifts the onset of photoabsorption of B_4C to higher energies with about 1 eV (approximately 0.03 nm lower wavelength) compared to amorphous and crystalline B (24). The origin of the B and B_4C based multilayer EUV reflectivity drop at shorter wavelengths is the increase of B absorption. The shift of the absorption on-set will lead to the shift of optimal wavelength. Our calculations yielded a difference in the optimal wavelengths of B and B_4C based multilayers of 0.02 nm or ~0.6 in eV, to be compared to the 1 eV shift found above. For estimation of the transmission of an EUV lithography system, we have calculated the integrated reflectivity of the convolution of a system consisting of ten single mirror normal incidence mirrors optimized for various wavelengths.

In Figure 4.2 we show the normalised integrated reflectivity calculated for LaN/B_4C and LaN/B using the measured optical constants. The graded color scale indicates the intensity of the Tb and Gd emission spectra(12) . All features of the single mirror peak reflectivity spectra are more pronounced on the 10 mirror integral reflectivity spectra. Figure 4.2 shows clearly that the wavelength of maximum throughput is at a slightly different wavelength: for the LaN/B material combination this is at λ=6.67 nm while for LaN/B_4C it is at λ=6.64 nm. These values are 0.02 and 0.01 nm higher compared to the optimal wavelength of a single B and B_4C based mirror respectively because of the influence of the wavelength dependent bandwidth on the integrated reflectivity.

Comparing the calculated transmission of a LaN/B multilayer coated ten mirror optical system to the source spectra we conclude that only the Tb source can be tuned to the optimal wavelength for this multilayer: λ= 6.67 nm. However, the difference of the optical throughput at λ= 6.67 nm and λ= 6.8 nm, where Gd can be used as a source material, is only ~20% for both the LaN/B_4C and LaN/B material combination. That means that the final choice of the wavelength may depend on the relative intensities of Tb and Gd radiation. Another factor, not taken into account in this paper, is the optical design of the lithographic system.

4.3 Normal incidence EUV reflectance

To test the influence of the real multilayer structure on the reflectivity profile, 150 period LaN/B_4C multilayer mirrors with different bi-layer thickness ranging from 3.3 to 3.5 nm have been deposited. The period variation allows determining the normal incidence peak reflectivity for the wavelength range from 6.5 to 7.2 nm. The measured maximum reflectivity values for different wavelength are shown in Figure 4.3. The reflectivity has been measured at the radiometry laboratory of the Physikalisch Technische Bundesanstalt (PTB) (25) using synchrotron radiation of the BESSY storage ring in Berlin, Germany. A maximum reflectance of 47.2% is observed at λ = 6.635 nm. The measured wavelength of maximum reflectivity is in good agreement with the calculated value of a perfect LaN/B_4C mirror described above.

To explain the obtained reflectivity we calculated the reflectance spectrum for each measured multilayer. The thus calculated spectra were fitted to the measurements and the peak reflectance of the fitted spectra is shown in Figure 4.3. The model used for these calculations consists of 150 periods of LaN and B_4C layers with different bi-layer thickness for each measured sample. Layer densities and interface roughness were the same for all samples. To have a proper fit of the reflectance dependency on the wavelength in Figure 4.3, the La density is reduced to 5 g/cm^3, while a B_4C density of 2.5 g/cm^3 has been used. The interface roughness, as described by the Debye–Waller factor, equals 0.7 nm for the LaN-on-B_4C interface and 0.4 nm for the B_4C-on-LaN interface. Modeling the reflectance profile turns out to be sensitive to the asymmetry of the interfaces but less sensitive to which of the interfaces is the larger one. Finally, for the wavelength region of 6.8 to 7.2 nm Figure 4.3 shows a slope that is steeper than in the calculations for the ideal multilayer represented in Figure 4.1. This is explained by the decreased optical contrast due to the lower than bulk density of the La in the LaN layers. Reflectivity improvement requires optimization of the deposition process in order to reduce the interface roughness as well as optimization of the nitridation process. This interface engineering challenge can be solved using reactive or inert ion or plasma treatment during La or B_4C layer deposition or ion/plasma post treatment of deposited layers.

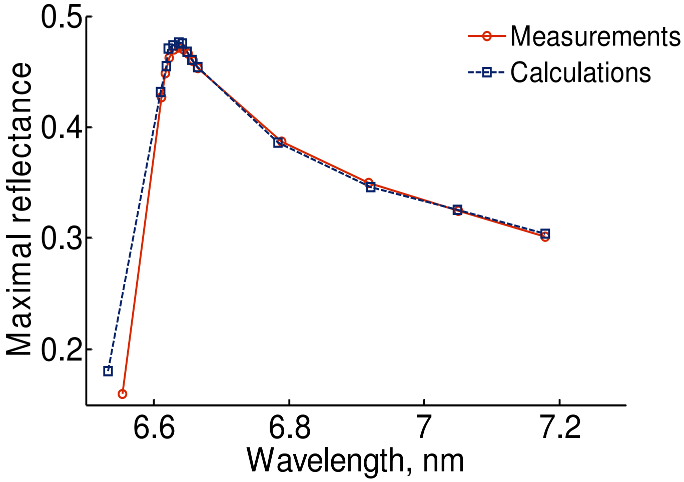

Figure 4.3Measured and fitted peak reflectivity for a 150 period LaN/B_4C multilayer mirror. The mirror had a lateral gradient in periodicity. The data points represent the maximum reflectance and corresponding wavelength at various positions on the mirror.

4.4 Conclusions

We have shown that for the evaluation of the performance of LaN/B and LaN/B_4C multilayer optics near the boron K absorption edge, the boron chemical state has to be taken into account. Experimentally determined optical constants were found to properly describe the optical response, as is demonstrated with an experimental verification for a LaN/B_4C multilayer mirror.

The calculated reflectivity of perfect multilayers, i.e. having zero interface roughness, shows that the optimal transmission of a B-based ten-mirror optical system is at a wavelength of 6.67 nm. For a wavelength larger than 6.67 nm there is a slight drop of reflectivity, while for smaller wavelengths the reflectance drops dramatically. Obviously, optimising the design and fabrication of multilayer mirrors for photolithography systems for wavelengths beyond the current Extreme UV requires a trade-off between the multilayer reflectivity response, the eventual source emission and photo resist absorption characteristics too.

4.5 References

1. Y. Platonov, J. Rodriguez, M. Kriese, E. Gullikson, T. Harada, T. Watanabe, and H. Kinoshita, "Multilayers for next generation EUVL at 6.X nm " *SPIE* **8076**(22), 1-9 (2011)
2. Y. Y. Platonov, L. Gomez, and D. Broadway, "Status of small d-spacing x-ray multilayers development at Osmic (Proceedings Paper)," *SPIE Conf. Proceedings* **4782**((2002)
3. A. M. Hawryluk and N. M. Ceglio, "Wavelength considerations in soft-x-ray projection lithography," *Appl. Opt.* **32**(34), 7062-7067 (1993)
4. Vinogradov A V, Brytov I A, Grudskii A Ya, Kogan M X, Kozhevnikov I V, and S. V. A, *Zerkal'naya rentgenovskaya optika (X-ray Mirror Optics)*, Leningrad: Mashinostroenie (1989).
5. E. Spiller, *Soft X-ray Optics*, SPIE optical Engineering press (1994).
6. T. Tsarfati, R. W. E. van de Kruijs, E. Zoethout, E. Louis, and F. Bijkerk, "Reflective multilayer optics for 6.7 nm wavelength radiation sources and next generation lithography," *Thin Solid Films* **518**(5), 1365-1368 (2009)
7. C. Montcalm, P. A. Kearney, J. M. Slaughter, B. T. Sullivan, M. Chaker, H. Pépin, and C. M. Falco, "Survey of Ti-, B-, and Y-based soft x-ray-extreme ultraviolet multilayer mirrors for the 2- to 12-nm wavelength region," *Appl. Opt.* **35**(25), 5134-5147 (1996)
8. J. M. Andre, P. Jonnard, C. Michaelsen, J. Wiesmann, F. Bridou, M. F. Ravet, A. Jerome, F. Delmotte, and E. O. Filatova, "La/B4C small period multilayer interferential mirror for the analysis of boron," *X-Ray Spectrom.* **34**(3), 203-206 (2005)
9. S. Andreev, M. Barysheva, N. Chkhalo, S. Gusev, A. Pestov, V. Polkovnikov, D. Rogachev, N. Salashchenko, Y. Vainer, and S. Zuev, "Multilayer X-ray mirrors based on La/B4C and La/B9C," *Technical Physics* **55**(8), 1168-1174 (2009)
10. J. Bosgra, E. Zoethout, A. M. J. van der Eerden, F. Boekhout, J. Verhoeven, R. W. E. van de Kruijs, A. E. Yakshin, and F. Bijkerk, "Structural properties of sub nanometer thick Y layers in EUV multilayer mirrors," *submitted to JAP* (2011)
11. T. Tsarfati, E. Zoethout, R. W. E. van de Kruijs, and F. Bijkerk, "Nitridation and contrast of B_4C/La interfaces and multilayers," *Thin Solid Films* **518,** (2010)

12. S. S. Churilov, R. R. Kildiyarova, A. N. Ryabtsev, and S. V. Sadovsky, "EUV spectra of Gd and Tb ions excited in laser-produced and vacuum spark plasmas," *Phys. Scr.* **80**(4), 6 (2009)
13. M. Fernández-Perea, J. I. Larruquert, J. A. Aznárez, J. A. Méndez, M. Vidal-Dasilva, E. Gullikson, A. Aquila, R. Soufli, and J. L. G. Fierro, "Optical constants of electron-beam evaporated boron films in the 6.8-900 eV photon energy range," *J. Opt. Soc. Am. A* **24**(12), 3800-3807 (2007)
14. R. Soufli, A. L. Aquila, F. Salmassi, M. Fernández-Perea, and E. M. Gullikson, "Optical constants of magnetron-sputtered boron carbide thin films from photoabsorption data in the range 30 to 770 eV," *Appl. Opt.* **47**(25), 4633-4639 (2008)
15. B. L. Henke, E. M. Gullikson, and J. C. Davis, "X-Ray Interactions: Photoabsorption, Scattering, Transmission, and Reflection at E = 50-30,000 eV, Z = 1-92," *Atomic Data and Nuclear Data Tables* **54**(2), 181-342 (1993)
16. E. Gullikson, "The Center for X-Ray Optics " (1995-2010).
17. J. F. Seely, Y. A. Uspenskii, B. Kjornrattanawanich, and D. L. Windt, "Coated photodiode technique for the determination of the optical constants of reactive elements: La and Tb," 63170T-63170T (2006)
18. G. Monac, D. Garoli, R. Frison, V. Mattarello, P. Nicolosi, M. G. Pelizzo, V. Rigato, L. Armelao, A. Giglia, and S. Nannarone, "Optical constants in the EUV Soft x-ray (5-152 nm) spectral range of B4C thin films deposited by different deposition techniques," *SPIE - Advances in X-ray/EUV Optics, Components, and Applications - SAN DIEGO - Int. Conf. Proceedings* (2006)
19. I. A. Makhotkin, E. Zoethout, E. Louis, A. M. Yakunin, S. Müllender, and F. Bijkerk, "Spectral properties of La/B - based multilayer mirrors near the boron K absorption edge," *Opt. Express* **20**(11), 11778-11786 (2012)
20. F. Mauri, N. Vast, and C. J. Pickard, "Atomic Structure of Icosahedral B4C Boron Carbide from a First Principles Analysis of NMR Spectra," *Physical Review Letters* **87**(8), 085506 (2001)
21. R. Lazzari, N. Vast, J. M. Besson, S. Baroni, and A. Dal Corso, "Atomic Structure and Vibrational Properties of Icosahedral B_{4}C Boron Carbide," *Physical Review Letters* **83**(16), 3230-3233 (1999)
22. D. W. Bullett, "Structure and bonding in crystalline boron and B 12 C 3," *Journal of Physics C: Solid State Physics* **15**(3), 415 (1982)
23. S. Koun, E. Shuichi, G. Shun-ichi, and K. Yukinobu, "Infrared study of amorphous B[sub 1 - x]C[sub x] films," *J. Appl. Phys.* **78**(5), 3392-3400 (1995)
24. I. Jiménez, L. J. Terminello, F. J. Himpsel, M. Grush, and T. A. Callcot, "Photoemission, X-ray absorption and X-ray emission study of boron carbides," *J. Electron Spectrosc. Relat. Phenom.* **101-103**(611-615 (1999)
25. F. Scholze, C. Laubis, C. Buchholz, A. Fischer, S. Ploeger, F. Scholz, H. r. Wagne, and G. Ulm, "Status of EUV reflectometry at PTB," *Pros. SPIE* **5751**(749-758 (2005)

5 Short period La/B and LaN/B multilayer mirrors for ~6.8 nm wavelength

In the first part of this chapter we experimentally show that contrast between the very thin layers of La and B enables close to theoretical reflectance. The reflectivity at 6.8 nm wavelength was measured from La/B multilayer mirrors with period thicknesses ranging from 3.5 to 7.2 nm at the appropriate angle for constructive interference. The difference between the measured reflectance and the reflectance calculated for a perfect multilayer structure decreases with increasing multilayer period. The reflectance of the multilayer with the largest period approaches the theoretical value, showing that the optical contrast between the very thin layers of these structures allows to experimentally access close to theoretical reflectance.

In the second part of the chapter we discuss the structure of La/B and LaN/B multilayers. This set of multilayers is probed by hard X-rays ($\lambda = 0.154$ nm) and EUV radiation ($\lambda = 6.8$ nm). The structure is reconstructed based on a simultaneous fit of the grazing incidence hard X-ray reflectivity and the EUV reflectivity curves. The reflectivity analysis of the La/B and LaN/B multilayer mirrors shows that the lower reflectance of La/B mirrors compared to LaN/B mirrors can be explained by the presence of 5 % of La atoms in the B layer and 63 % of B in La layer.

After multi-parametrical optimization of the LaN/B system, including the nitridation of La, the highest near normal incidence reflectivity of 57.3% at 6.6 nm wavelength, has been measured from a multilayer mirror, containing 175 bi-layers. This is the highest value reported so far.

5.1 Introduction

One of the possible wavelengths for the next generation EUV lithography is around 6.8 nm[1-4]. To maximize the multilayer reflectance it is required to select materials with the highest possible optical contrast and the lowest possible absorption for the selected wavelength. The most commonly used multilayer material combinations for normal incidence reflectance at this wavelength, just above the boron K_α absorption edge, are Mo/B_4C or La/B_4C [1, 5].

Due to their good thermal stability, Mo/B_4C multilayer mirrors are often considered for applications using high power soft X-ray light sources, for example X-ray free electron lasers[6]. However, according to their bulk optical properties, La-based multilayers show a higher reflectance than Mo-based multilayers and are therefore better candidates for applications that require a high photon transmission such as EUV lithography. La/B_4C multilayer mirrors have also been studied for application in X-ray fluorescence spectroscopy [7], in particularly for boron detection [8].

To increase the multilayer reflectivity further, B_4C should be replaced by boron since this is the optically preferable material in combination with La. The boron rich compound B_4C has been selected previously over boron because of its higher electrical conductivity[9] which simplifies deposition with commonly used DC magnetron sputtering techniques. Boron, being a semi-conductor at room temperature, is usually deposited by RF magnetron sputtering, but DC magnetron sputtering sources can be employed for boron when the target is heated above 400^0C [10], where the conductivity improves sufficiently.

Normal incidence reflectance calculations made with IMD [11], using measured optical constants for B [12] and B_4C [13], assuming a typical 0.3 nm rms roughness value for each interface and 200 period multilayers, show that La/B can reflect 7% more at 6.8 nm wavelength compared to La/B_4C. Reflectivity gain by replacing B_4C by B is experimentally demonstrated for 50 period La/B_4C and La/B multilayers with a period of 3.5 nm showing 7% and 10% normal incidence reflectance at λ= 7 nm respectively.

However, replacement of B_4C with a more boron rich boron-carbide is not always beneficial for reflectivity. Andreev et. al. [14] reported 38% reflectivity for La/B_9C multilayer mirrors, lower than the 44% reflectivity reported for La/B_4C in the same work. This boron-carbide example shows that differences in growth properties of the different materials can have a large impact on optical performance and may negate any theoretically expected improvements.

In the first part of this chapter we discuss the potential of the optical contrast of the La/B material combination to reach high EUV reflectance by analysing the measured EUV reflectivity from multilayer stacks with different period thickness for various angles of incidence.

The second part of the chapter describes the current state of our La/B-based multilayer mirrors. It has been reported that nitridation of La in La/B_4C multilayer mirrors increases the multilayer reflectivity [2]. This increase is assumed to be caused by the nitrogen passivation of the lanthanum preventing or mitigating lanthanum-boride formation. This can also be applied when B is used instead of B_4C. We will present the near normal incidence reflectivity and analysis of the structure of La/B and LaN/B stacks deposited for normal incidence of 6.8 nm EUV radiation. Here we analyse the multilayer structures in order to study the structural effects of the lanthanum nitridation in B based multilayers. We compare two ways of La nitridation: N-ion post treatment of the La layers and reactive magnetron sputtering of La using a N_2 and Ar gas mixture.

5.2 Optical contrast between La and B layers

The reflectivity loss caused by interface roughness or intermixture can be described by multiplying the reflectivity from an interface without roughness by the Debye Waller-like correction factor $\exp(-q^2\sigma^2)$, were q is the scattering vector equal to $4\pi\cos(\theta)/\lambda$ (θ is angle of incidence (AOI) with respect to surface normal, λ is the X-ray wavelength) and σ is an effective interface thickness. According to Bragg's law in its basic form, so without taking the material optical constants into account, the scattering vector q is for the first order reflection equal to $2\pi/\Lambda$, where Λ is the multilayer period. This indicates that for multilayers with a larger period thickness and the same roughness σ, a lower reflectance loss due to roughness can be expected. Therefore, increasing the period thickness and measuring the reflectivity at a more grazing incidence angle, the effect of interfaces on the EUV reflectivity is minimized and the optical potential of the material combination can be assessed.

In this section we will discuss the reflectance of 40 period La/B multilayer stacks with different period thicknesses. To avoid run-to-run variations in the deposition process, all samples have been deposited in one deposition run, using a vapour-mask to vary the deposition flux. The mask enables the deposition of multilayer stacks with periods ranging from 7.8 nm to

3.2 nm. To minimize shadowing effects and simplify the mask design the electron beam evaporation technique has been used. Deposition is controlled using in-situ soft X-ray reflectivity of C-K radiation from the sample in the centre of the substrate holder [15].

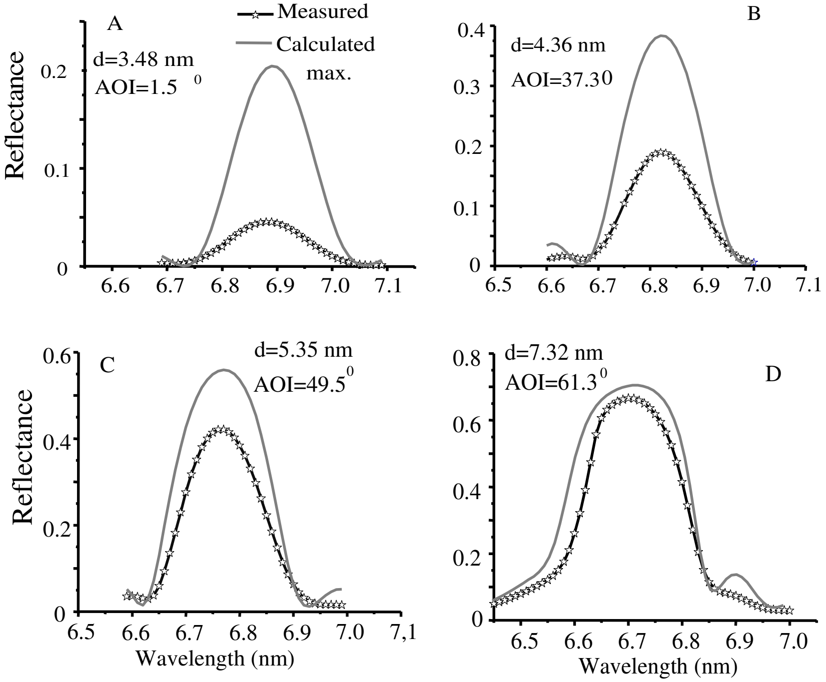

Figure 5.1 Measured (markers) and simulated (lines) EUV reflectivity for e-beam deposited 40 period La/B multilayers with different periods. Simulations are performed using the parameters indicated in table 5.1.

The multilayers have been characterized using at-wavelength reflectometry at the facility of the Physikalisch Technische Bundesanstalt (PTB) in Berlin [16] using radiation of the electron storage ring BESSY. The angle of incidence, given with respect to the surface normal, is selected to have the maximum reflectance at 6.8 nm for each sample. The results are presented in table 5.1 and plotted in Figure 5.1 and show that the measured reflectivity of the multilayer stacks increases with increasing period thickness. There are multiple factors for the observed reflectance increase. For instance the increase in reflectivity for the s-polarized EUV light with increasing angle of incidence. Another factor is that for off normal incidence reflectance fewer layers contribute to the reflected intensity. For example, at 61.3 degrees from normal incidence only 40 periods contribute to the reflectance, compared to the more than 160 periods that are needed to saturate the reflectance at 1.5 degree. Therefore we compare the measured reflectivity to the theoretical maximum reflectivity calculated for a model of 40 periods La/B without interface roughness, using bulk values for La and B densities and the as-deposited ratio of the La and B layer thickness.

Reconstruction of the multilayer structure based on EUV reflectivity data only is impossible because of the large correlation between roughness, layer thickness ratios and density. In order to get an indication for the roughness of our samples, the roughness of the top surface has been measured with an atomic force microscope, indicating no significant differences. Furthermore, we are able to use the same model (not presented here), including equal interface parameters, to fit the measured reflectivity of the multilayers with different period thicknesses. This, together with the AFM measurements suggests that there is no significant structural difference between the different stacks.

The decrease of the difference between the maximum achievable reflectivity and the measured values for more grazing angles of incidence is explained by the smaller ratio of the layer roughness or intermixed zone compared to the total period thickness. The important result of our analysis is that close to theoretical reflectance values can be obtained experimentally as shown in Figure 5.1(D), confirming that La and B have sufficient optical contrast to achieve high reflectance providing the multilayer interface structure can be improved.

Figure	Λ, nm	AOI, degrees	R, %	$R^{sim.}$, %	Wave-length, nm	AFM rms roughness, nm
5.1 A	3.49	1.5	4.5	20	6.89	0.3±0.05
5.1 B	4.36	37.3	18.5	38	6.82	
5.1 C	5.35	49.5	42.1	56	6.76	
5.1 D	7.32	61.3	66.5	72	6.71	

Table 5.1 .Summary of measured and calculated reflectance of La/B multilayer mirrors with period thicknesses from 3.45 to 7.25 nm at indicated angles of incidence.

5.3 La/B and LaN/B multilayer structures

5.3.1 Experimental

In this section we analyze the composition of a La/B and two differently produced LaN/B multilayer mirrors. The stacks are deposited using the magnetron sputtering deposition method described by Yakshin et al. [17]. Two different methods are used to nitridate the La layers: reactive magnetron sputtering of La in a mixture of Ar and N_2 (indicated by La(N)/B) and post treatment of the La layers by N_2-ions[2] (indicated by La/N/B). For our structural analysis we have deposited 50 bi-layers instead of the 175 required for maximum normal incidence EUV (NIER) reflectance because 50 period stacks suffer less from period variations. The period thickness is optimized for reflectance at 6.8 nm wavelength, close to but sufficiently far from the B-K absorption edge to avoid edge effects in the NIER curve.

The common way to reconstruct the multilayer mirror structure is to fit the grazing incidence hard X-ray reflectivity (GIXR) data, measured typically with $CuK_{\alpha1}$ radiation. Fitting procedures assume minimization of a merit function by variation of the model parameters: interface roughness, layer density and layer thickness. However, due to the large amount of variable parameters for multilayer structures, the data fit will be complex. Moreover, it is impossible to prove that the obtained fit is the unique solution to the problem. Combining GIXR and NIER fits increases the consistency of the fits not only because of the increasing amount of experimental data, but also because of the different optical response of the materials to the used hard and soft X-rays. Both measurements are sensitive to the electron density profiles of multilayer periods, but GIXR is less sensitive to the

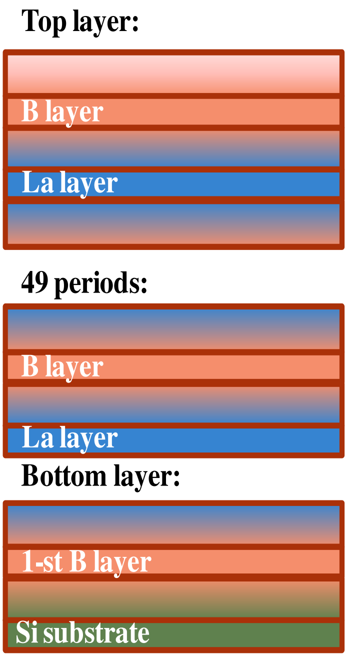

Figure 5.2 The scheme of the model for grazing incidence hard X-ray reflectivity and normal incidence EUV reflectance data fitting.

exact atomic composition of the layer (particularly the presence of lanthanum in boron) and the fit suffers less from correlation between structure parameters. Because of the large optical contrast for EUV light between spacer (here B) and reflector (here La) material, the NIER is sensitive to the atomic composition of the layers, particularly for the spacer layer. We first performed a GIXR data fit, minimizing χ^2 for the GIXR data to generate the starting conditions for the simultaneous fits of GIXR and NIER that minimize the sum $\chi^2_{\mathrm{GIXR}} + \chi^2_{\mathrm{NIER}}$.

The data fit was carried out using the model of a multilayer structure presented in Figure 5.2, assuming the multilayer to consist of a B-layer on a Si substrate, N-1 identical periods with N being the number of periods, and finally one bi-layer on the top of the stack. The substrate surface roughness, parameters of the first boron layer, period bi-layer and top bi-layer can be varied separately. The top layer and the substrate are mostly responsible for the reflectivity features observed between the Bragg diffraction peaks in the GIXR curves (Figure 5.3) and our model should be able to fit this. Physically, parameters of the first boron layer and top period can be different from the periodic layers because of contact to substrate and air respectively. For each layer the layer thickness, density and interface thickness and the atomic composition can be varied during the fit. The interface roughness/diffusion regions are described by dividing the interface area in thin sub-layers with thickness of less than 0.1 nm, creating a linear profile in the optical contrast. This allows bypassing the discussion about the validity of the Debye-Waller or the Nevot-Crosse approximation to describe the GIXR and NIER data.

Measurements and calculations of GIXR using the results of the simultaneous fits are presented in Figure 5.3. To demonstrate the fit quality, residuals calculated from the fit and data for each measured point are displayed in Figure 5.4 together with the value of χ^2. The small difference in the χ^2 value indicates that the fits can be considered of equal quality. All Bragg maxima are described equally well and the difference in χ^2 values are mainly due to the regions in between the Bragg peaks where the top-bottom of the complete stack and layer aperiodicity are the major factors. The measured NIER spectra as well as the results of the simultaneous fit with the data of Figure5.3 are plotted in Figure5.5 showing a very good agreement. It should be noted that adding the layer stoichiometry to the fitting variables is vital to enable high quality simultaneous fitting of GIXR and NIER. Like in EUV reflectivity modelling in part one, measured La[18] and B[12] optical constants have been used.

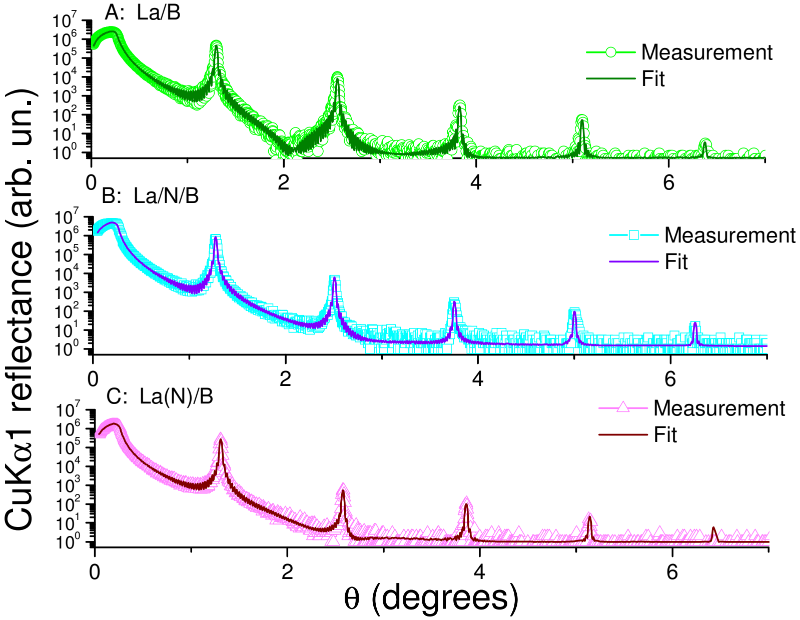

Figure 5.3 Measured and calculated grazing incidence Cu-$K_{\alpha l}$ reflectivity curves for La/B, La/N/B and La(N)/B multilayers.

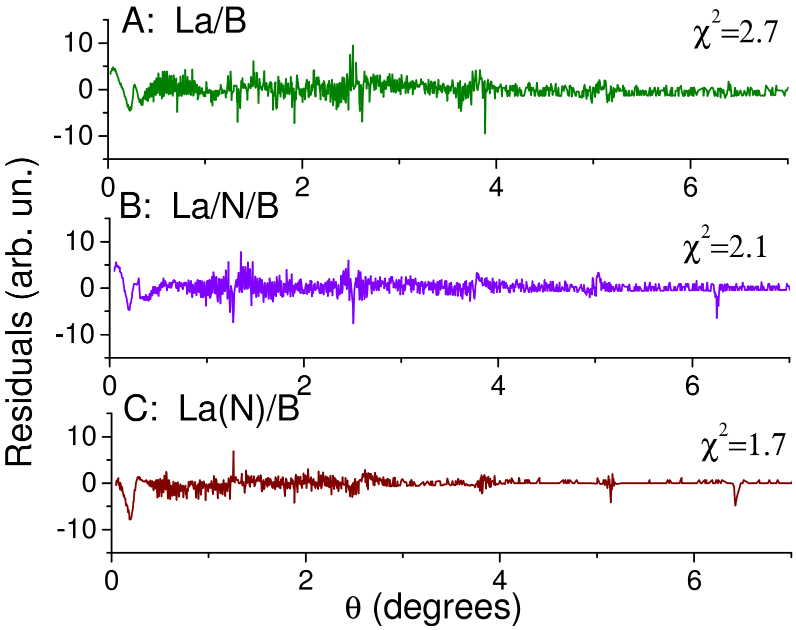

Figure 5.4 Residuals between Cu-$K_{\alpha l}$ measured and calculated data presented in Figure 5.3.

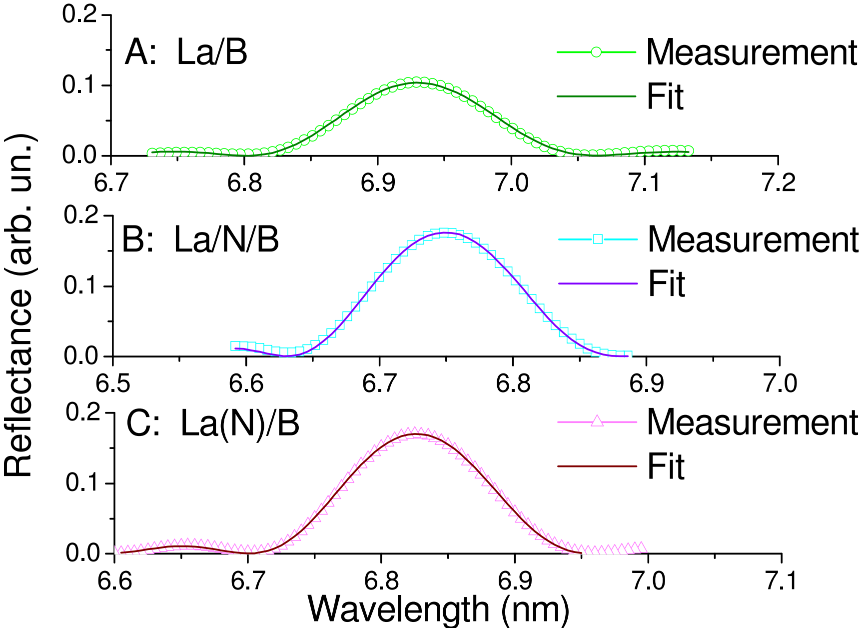

Figure 5.5. Measured and calculated normal incidence EUV reflectivity spectra for 50 period La/B, La/N/B and La(N)/B multilayer stacks.

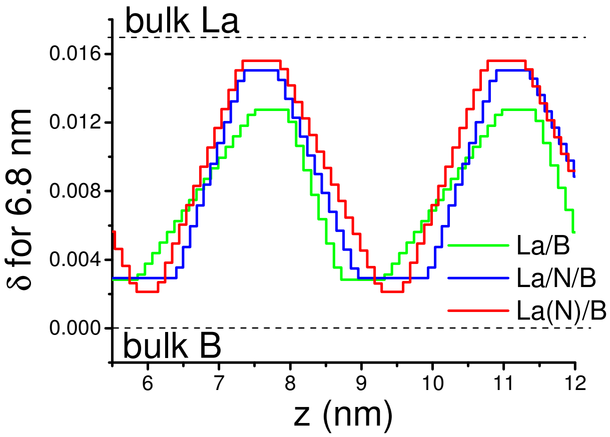

Figure 5.6 Reconstructed optical profile for La/B, La/N/B and La(N)/B multilayer stacks calculated for 6.8 nm wavelength and presented as δ=1-n where n is the real part of the dielectric permittivity.

5.3.2 Discussion

The results of the simultaneous fit of GIXR and NIER data of the La/B, La(N)/B and the La/N/B multilayers are summarized in table 5.2 and in Figure 5.6 that displays the reconstructed optical contrast profiles of these three multilayers. These profiles are represented by δ (δ=1 – n with n being the real part of the optical constants) and are calculated for 6.8 nm wavelength.

Figure 5.6 shows that La/B multilayer has the lowest optical contrast which results in a reflectance of only 10.5 % (Figure 5.5). Furthermore, table 5.2 shows that the B layer in the La/B stack has high density of 2.9 g/cm^3 compared to its bulk value of 2.1 g/cm^3. This can be explained by the presence of 5 at.% La in the B layer. The La layer density of 5.2 g/cm^3 is rather low compared to the 6.17 g/cm^3 for bulk material, most likely caused by 63 at% of B in the La layers (see table 5. 2). The huge amount of B in La layer can be explained by dramatic intermixing of La and B. However, one should be careful with the obtained absolute value since the fit is not very sensitive to the B in La concentration. The La contamination in the B layer has a more dramatic effect on the optical contrast than B in La, therefore, the fit is much more sensitive to the presence of La in B than B in La. The interface asymmetry that is detected indicates that the B-on-La interface region is thicker than the La-on-B interface, which can be explained by 3-dimensional growth of the La layer leading to a thicker interface region when B grows on it. Table 5.2 shows that only 30% of the La/B period consists of layers with constant atomic composition and density, or in other words is not a part of the interface region. This also shows the relatively large intermixing.

The reconstructed profiles for both LaN/B stacks (Figure 5.6) confirm that passivation of La with nitrogen, either by post N-ion treatment or by the reactive sputtering of La, increase the optical contrast by preventing the La-B diffusion or improving the layer growth properties. However for both multilayers the optical contrast is still lower than for LaN and B layers with bulk properties. According to table 5.2 the density of the LaN layer in both multilayers is lower than the bulk value for the stoichiometric LaN which is 6.7 g/cm^3. This means that the LaN layer should either contain some B or pores to explain the layer density. Because of the small difference between boron and nitrogen optical constants compared to La, the fit is not sensitive to the exact atomic composition of the LaN layer as well as the presence of B in LaN layer. In the initial fitting model the atomic composition of the nitrided lanthanum layer was selected as LaN. During the fit it remains as initially assumed, LaN, for both stacks, La/N/B and La(N)/B, although the composition coefficients were free to vary.

Table 5.2 suggests that in the La/N/B multilayer the boron layers contain 21 at.% of N versus 16 at.% in the La(N)/B multilayer, resulting in a higher than bulk density. This can easily be understood in both cases: although the N-ion treatment in the La/N/B multilayer takes place only after deposition of the La N-ions can easily penetrate the La and penetrate in the B-layer because of the low La thickness. This is confirmed by TRIM calculations for 150 eV N_2. In the case of reactive magnetron sputtering for La(N) deposition the plasma creates also nitrogen ions and radicals that can interact with the sample surface as soon as the plasma is created. This creates boron-nitride simultaneously with the first arriving lanthanum particles, potentially changing growth conditions and modifying all important parameters for layer growth. The fact that La(N)/B has a higher optical contrast than La/N/B can be explained by better growth conditions of LaN on B than in the case of La on B.

Sample	Layer thick-ness, nm	Interface linear transition width, nm (on top of the layer)	Density, g/cm^3	Layer compound stoichiometry, at %		
				La	B	N
La/B: R 10.5% @6.92 nm						
B layer	0.6	0.7	2.9	5	95	
La layer	0.5	1.6	5.2	37	63	
La/N/B R:17.5% @6.75 nm						
B layer	1.0	1.1	2.5	0	79	21
La/N layer	0.5	1.0	5.1	50	0	50
La(N)/B R:17% @6.82 nm						
B layer	0.3	1.4	2.4	0	84	16
La(N) layer	0.5	1.2	5.3	50	0	50

Table 5.2 The summary of the structural parameters for La/B, La/N/B and La(N)/B multilayer reconstructed using simultaneous grazing incidence X-ray reflectivity and normal incidence EUV reflectivity fits.

Both LaN/B multilayers do not show the asymmetry of the interfaces observed in the La/B stack. However no significant reduction of the total interface region is observed. The analysis of the La/N/B stack shows that the thickness of the layers with constant atomic composition and density is increased to about 40% of the period thickness but the La(N)/B multilayer has an even smaller non-interface region than the La/B multilayer. Comparing the two techniques to produce LaN, the only difference observed, is that it turns out that the reactive magnetron sputtering produces a lower amount of nitrogen content in the boron layers at the expense of a slightly larger interface width. The smaller thickness of the interface regions in the La/N/B multilayer compensate the effect of the lower optical contrast compared to the La(N)/B multilayer and as a result both La/N/B and La(N)/B multilayers show comparable near normal incidence EUV reflectance for the analysed 50 period multilayer mirrors. The next step in the development of the stack deposition technology could be the combination of the reactive La sputtering with N-ion post treatment.

5.4 High reflectance coatings

In order to demonstrate high reflectance for lanthanum-boron multilayers, the best candidates from the previous set have been scaled up. La(N)/B and La/N/B multilayer mirrors consisting of 175 periods have been deposited to evaluate the achievable normal incidence reflectance around 6.7 nm wavelength. The EUV reflectivity measurements have been performed, similar to measurements for 50 period coatings, at 1.5 degree of normal using s-polarized light.

The measured reflectivity results are presented in Figure 5.7 together with simulations based on the model parameters obtained for the 50 period multilayer described in the previous section. No additional fits have been performed. The only difference with the previous section is the number of periods and the period thickness that had to be slightly scaled to match the wavelength of ~ 6.65 nm. It should be noticed that the model reconstructed for 50 period coating does not take any aperiodicity or roughness evolution during the multilayer growth into account.

Figure 5.7 shows that a reflectance for La/N/B of 53 % has been measured versus 57.3 % for the La(N)/B multilayer mirror. The measured reflectivity is in both cases smaller than the 60% value predicted by the simulations. The reflectance curve of the La/N/B multilayer (Figure 5.7 a) shows a significantly larger width than the calculated curve as well as the measurement of the La(N)/B multilayer (Figure 5.7 b). This increase in the La/N/B reflectance peak width and the slightly larger Kiessig fringe oscillations can be simulated by a decrease in the number of periods from 175 to 145, hinting more in the direction of aperiodicity in the stack. The predicted reflectance is met best by the

La(N)/B multilayer mirror indicating that the La(N)/B multilayer deposition has lower aperiodicity and no significant evolution of interface roughness. The higher aperiodicity of La/N/B multilayer can be explained by the difference in the deposition process. The post N-ion treatment is an additional step in the deposition process and may cause extra instability of the growth process that is best visible for a coating with large number of periods.

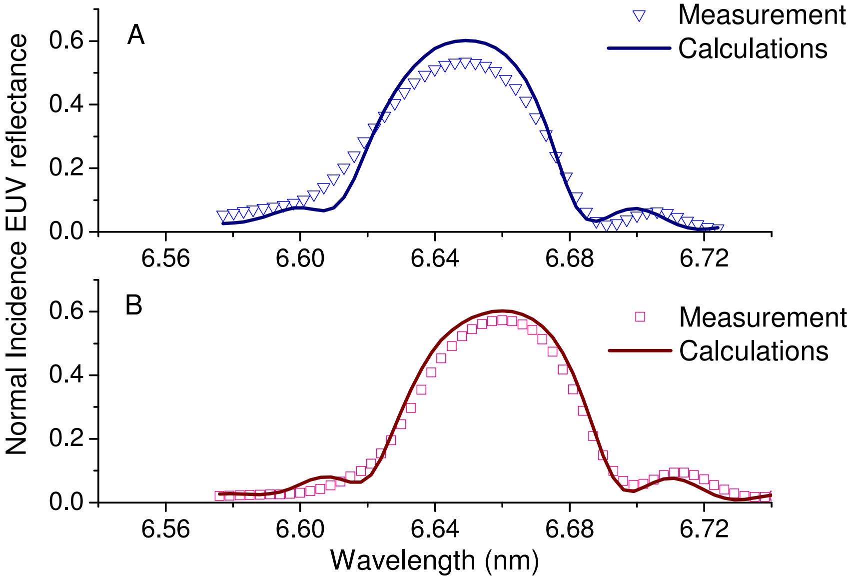

Figure 5.7 Normal incidence EUV reflectivity spectra for 175 period La(N)/B (A) and La/N/B (B) multilayer mirrors measured and calculated using models reconstructed for 50 period stacks.

However, in both cases the difference between the obtained and predicted reflectance is not dramatic and optimisation of the deposition technology should be able to correct for this.

5.5 Conclusions

Experiments with large period multilayers for off normal reflectance of 6.8 nm radiation have demonstrated that the material combination of La with B shows sufficient optical contrast to obtain almost theoretical reflectance values if the influence of interface roughness can be reduced.

Analysis of short period La/B multilayer structures for normal incidence reflectance of 6.8 nm light has revealed that the multilayer has a low optical contrast that is most likely caused by intermixing between the layers. In order to prevent this intermixing two techniques of nitridation of La, namely post N-ion treatment of the thin La layer and reactive La sputtering in a N_2 atmosphere have been applied to deposit LaN/B multilayers. The nitridation of La in both cases increases the optical contrast between La and B significantly and consequently increases the EUV reflectivity. The nitridation does however not change the total width of the interfaces, leaving ample room for further improvements.

The optical contrast of LaN/B multilayer stacks is also limited by the presence of N atoms in the B layers and should be reduced by further improvement of the nitridation process. The highest normal incidence reflectivity of 57.3 % at 6.65 nm was measured from the 175 period La(N)/B multilayer stack. The measured reflectivity is slightly less than calculated values of 60% that is based on the reconstructed multilayer structure. The difference can be explained by a minor error in periodicity or roughness growth for large number of periods, but no major changes of structure caused by the multilayer growth process is detected.

5.6 References

1. Platonov, Y.Y., L. Gomez, and D. Broadway, *Status of small d-spacing x-ray multilayers development at Osmic (Proceedings Paper).* SPIE Conf. Proceedings, 2002. **4782**.
2. Tsarfati, T., et al., *Nitridation and contrast of B_4C/La interfaces and multilayers.* Thin Solid Films, 2010. **518** p. 7249-7252.
3. Andreev, S., et al., *Multilayer X-ray mirrors based on La/B4C and La/B9C.* Technical Physics, 2009. **55**(8): p. 1168-1174.
4. Makhotkin, I.A., et al., Spectral properties of La/B - based multilayer mirrors near the boron K absorption edge. Opt. Express, 2012. **20**(11): p. 11778-11786.
5. Tsarfati, T., et al., Reflective multilayer optics for 6.7 nm wavelength radiation sources and next generation lithography. Thin Solid Films, 2009. **518**(5): p. 1365-1368.
6. Barthelmess, M. and S. Bajt, Thermal and stress studies of normal incidence Mo/B4C multilayers for a 6.7 nm wavelength. Appl. Opt., 2011. **50**(11): p. 1610-1619.
7. Michaelsen, C., et al. La/B4C multilayer mirrors for x-rays below 190 eV. in Proceedings of SPIE - The International Society for Optical Engineering. 2001.
8. Andre, J.M., et al., La/B4C small period multilayer interferential mirror for the analysis of boron. X-Ray Spectrometry, 2005. **34**(3): p. 203-206.
9. Domnich, V., et al., *Boron Carbide: Structure, Properties, and Stability under Stress.* Journal of the American Ceramic Society, 2011. **94**(11): p. 3605-3628.
10. Gushenets, V.I., et al., Boron ion source based on planar magnetron discharge in self-sputtering mode. Review of Scientific Instruments. **81**(2).

11. Windt, D.L., IMD - Software for modeling the optical properties of multilayer films. Computers in Physics, 1998. **12**(4): p. 360-370.
12. Fernández-Perea, M., et al., Optical constants of electron-beam evaporated boron films in the 6.8-900 eV photon energy range. J. Opt. Soc. Am. A, 2007. **24**(12): p. 3800-3807.
13. Soufli, R., et al., Optical constants of magnetron-sputtered boron carbide thin films from photoabsorption data in the range 30 to 770 eV. Appl. Opt., 2008. **47**(25): p. 4633-4639.
14. Andreev, S.S., et al., *Multilayered mirrors based on La/B4C(B9C) for X-ray range near anomalous dispersion of boron (lambda approximate to 6.7 nm).* Nuclear Instruments & Methods in Physics Research Section a-Accelerators Spectrometers Detectors and Associated Equipment, 2009. **603**(1-2): p. 80-82.
15. Louis, E., et al., Nanometer interface and materials control for multilayer EUV-optical applications. Progress in Surface Science, 2011. **86**(11): p. 255-294.
16. Scholze, F., et al., *Status of EUV reflectometry at PTB.* Pros. SPIE 2005. **5751**: p. 749-758.
17. Yakshin, A.E., et al., Enhanced reflectance of interface engineered Mo/Si multilayers produced by thermal particle deposition. Proc. of SPIE 2007. **6517**: p. 65170I-1 - 65170I-9.
18. Seely, J.F., et al., Coated photodiode technique for the determination of the optical constants of reactive elements: La and Tb. 2006: p. 63170T-63170T.

6 Determination of the density of ultrathin La films in La/B_4C layered structures using X-ray standing waves

Using simultaneous analysis of both the grazing incidence X-ray reflectivity (GIXR) and the angular dependent fluorescence yield from ultrathin layer structures, the densities of thin La and LaN layers of 2-6 nm thickness enclosed by B_4C layers have been determined with approximately 5% precision. The density of the La layer in these systems is found to be reduced to the bulk La value. This is explained by LaB_6 interlayers formation. The density of LaN layers were similar to the bulk LaN value, which favours this compound as the most energetically stable in LaN/B_4C layered systems.

6.1 Introduction

The continuous reduction of the printed feature size in modern semiconductor devices has required a shift to lower values of the operational wavelength in the lithographic process. Reducing this wavelength requires the development of new multilayer reflective coatings for the optics. For 6.7 nm, the most promising mirrors are multilayers[1] where the reflection layer is based on La and the spacer layer on boron or boron-rich compounds such as B_4C. For normal incidence reflectance multilayer mirrors, the required period is about 3.4 nm, so the individual layer thickness should be below 2 nm. Although model simulations for a 250 period La/B_4C multilayer would suggest a maximum reflection of 70% for 6.7 nm wavelength, the maximum reflectivity value reported in literature[2,3] is slightly above 40%. One of the parameters that may limit EUV reflection from these mirrors is the density of the La layer. While there are publications reporting first results [2, 4], [5, 6] of 6.7 nm reflectance from La/B_4C mirrors, structural properties of this system are not sufficiently studied. For instance, the published La densities used in multilayer descriptions vary from 5 g/cm^3 [6] up to 6.17 g/cm^3 [3]. In this paper we study the density of a very thin La film and explain the reduction of the film density and the effect of nitrogen treatment of the film.

In general, different techniques are available for the determination of thin film densities. The easiest way to probe the density is by analysis of the critical angle of total external reflection from a single film deposited on a substrate. This technique however has strong limitations: the film to be analyzed should be sufficiently thick (normally thicker than 100 nm) to provide a reliable solution. The determination of the density is also strongly dependent on the alignment accuracy [7] of the experiment. A misalignment of 0.005°, for example, results in a 5% density variation. Although geometry induced errors could be partially corrected by a multiple wavelength approach [8, 9], such experiments are impractical due to their complex nature. In addition to the experimental challenges, also the nature of the thin film to be investigated should be taken into account. For highly reactive materials, a single thin film will immediately react with its environment (e.g. substrate interaction, surface oxidation, etc), complicating the analysis even further.

A more promising method to determine the density of the thin film is simultaneous analysis of its specular X-ray reflection and its angular dependant fluorescence yield using a specially designed layer structure.

6.2 Experiment and simulations

The multilayers under study consist of an alternating stack of La and B_4C. The La density is a critical parameter and depends not only on the thickness of the layer, but also on the material and structure of the adjacent layers. Therefore, the goal of this research was to determine the density of such a thin La layer in between two B_4C layers. In the current study, we designed a waveguide [10-12] structure consisting of [2 nm Cr / 30 nm B_4C / xx nm La / 10 nm B_4C] on a Si substrate. Cr is preferable as top layer because it has a critical angle similar to La, which is essential for formation of waveguide modes and because of the energy of the fluorescent radiation that can spectrally be separated from the La signal. The Cr layer can thus be considered as a marker layer. The thickness of the first B_4C spacer was adjusted to 30 nm to be able to observe at least 2 waveguide modes. A calculation of the angular dependant electric field distribution in a sample with 6 nm La is presented on Figure 6.1. The calculations were carried out by using recursive equations with Fresnel coefficients for CuKα wavelength using atomic scattering factors from the CXRO database[13].

Measuring the fluorescence yield angular dependence from the top Cr layer, one can observe the intensity of the XSW field in a waveguide. The angular dependence of Cr fluorescence yield has been calculated for various La layer densities (Figure 6.2). Reduction of the La layer density by 10% will lead to a reduction of the second mode (T2) amplitude by 14%. The error in this type of fluorescence measurements is typically in the order of 5 %, which enables a La density determination with an accuracy better than 5% To achieve this accuracy, systematic errors like beam footprint and detector aperture have been corrected. It should be noted that this method of determining the La density does not suffer from sample misalignment such as in “traditional” critical angle analysis, because the information is actually obtained from the amplitude of the fluorescence oscillations.

The density of Cr can be determined by analysis of its first oscillation (T1 in Figure 6.2). The first oscillation of the Cr x-ray fluorescence intensity is determined by the first waveguide mode formation which is mostly sensitive to the density of top layer, namely Cr. All other oscillations are the results of higher order mode formation and their intensity depends on the densities of both the La and the Cr layers. Thus the Cr layer density can be fixed in the fit and the La layer density can then be extracted. The simulations show that most relevant information can be obtained from analyzing the grazing incidence angular region between 0.25 and 0.45 degrees.

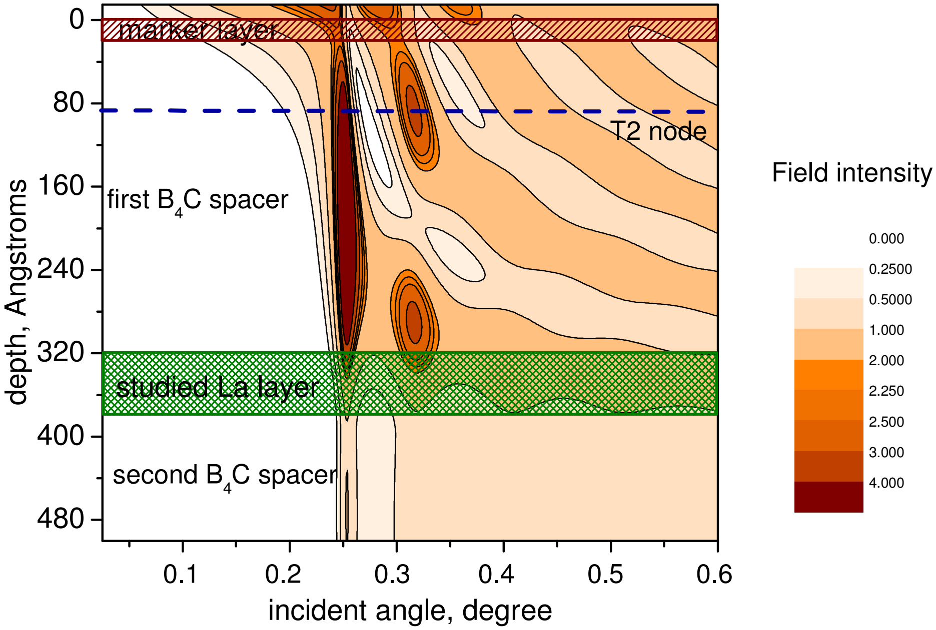

Figure 6.1 Calculation of angular dependent X-ray standing wave.

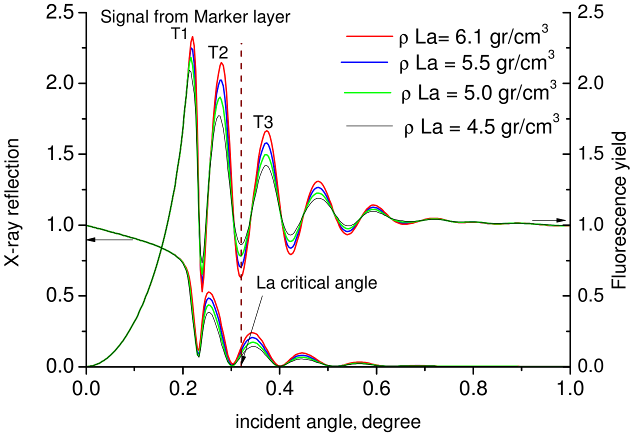

Figure 6.2 Calculated angular dependencies of the fluorescence yield from the marker layer and specular X-ray reflection.

A further step in the density determination technique described can be made by probing the waveguide mode intensity. The electric field in a waveguide is resonance enhanced, so its intensity variations will also be enhanced. Measuring the fluorescence yield from a second ultrathin marker layer placed in a position of the T2 node (dashed dark blue line on Figure 6.1); one can probe the waveguide node intensity. Calculations (not shown here) show that 10% La density variation can lead to 30% variation of this marker layer fluorescence intensity modulated by the T2 waveguide mode.

6.3 Results and discussions

In previous work, using in vacuum X-ray photo electron spectroscopy (XPS) analysis carried out on two-layer La/B_4C and B_4C/La systems, Tsarfati et.al.[5] have found that for B_4C-on-La an approximately 1.5 nm LaB6 mixed interface layer is formed. In the case of La-on-B_4C, the interface layer was determined to be 0.5 nm LaB_6. This suggests that when considering a 2 nm thin La layer deposited between B_4C layers, the entire La layer could form a more or less homogenous LaB_6 layer which will lead to a reduced density with respect to pure La. Thus, an increased density is expected for thicker La layers, where "bulk" La remains after interface formation. Furthermore we consider the case for LaN films, where the La layer was passivated with nitrogen to reduce the chemical interaction with the B_4C layers[3].

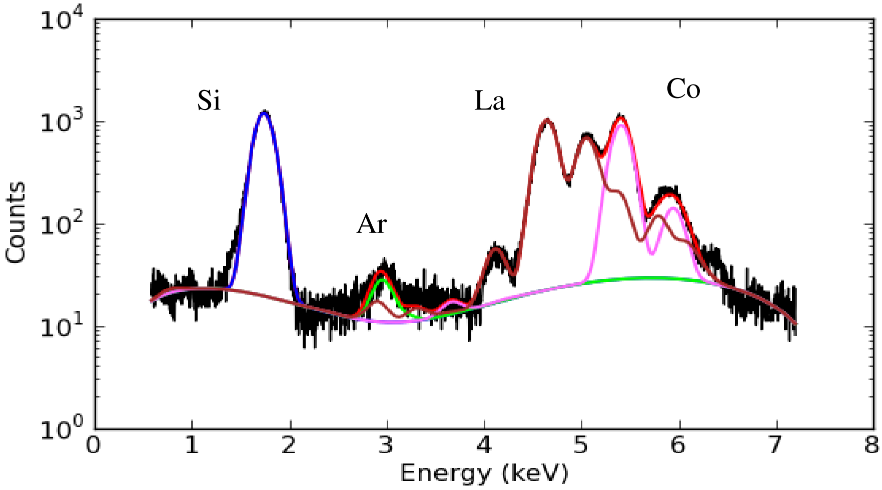

Figure 6.3 Fit of fluorescence spectra.

In this study, we consider three waveguide structures with xx=2 nm La (sample A), xx=6 nm La (sample B), and xx= 6 nm LaN (sample C). The La layers were deposited with a modified DC magnetron sputtering system, using the setup described in ref [14]. LaN was prepared by N-ion assisted deposition as described in ref [3]. Cr and B_4C were deposited at room temperature using electron beam deposition.

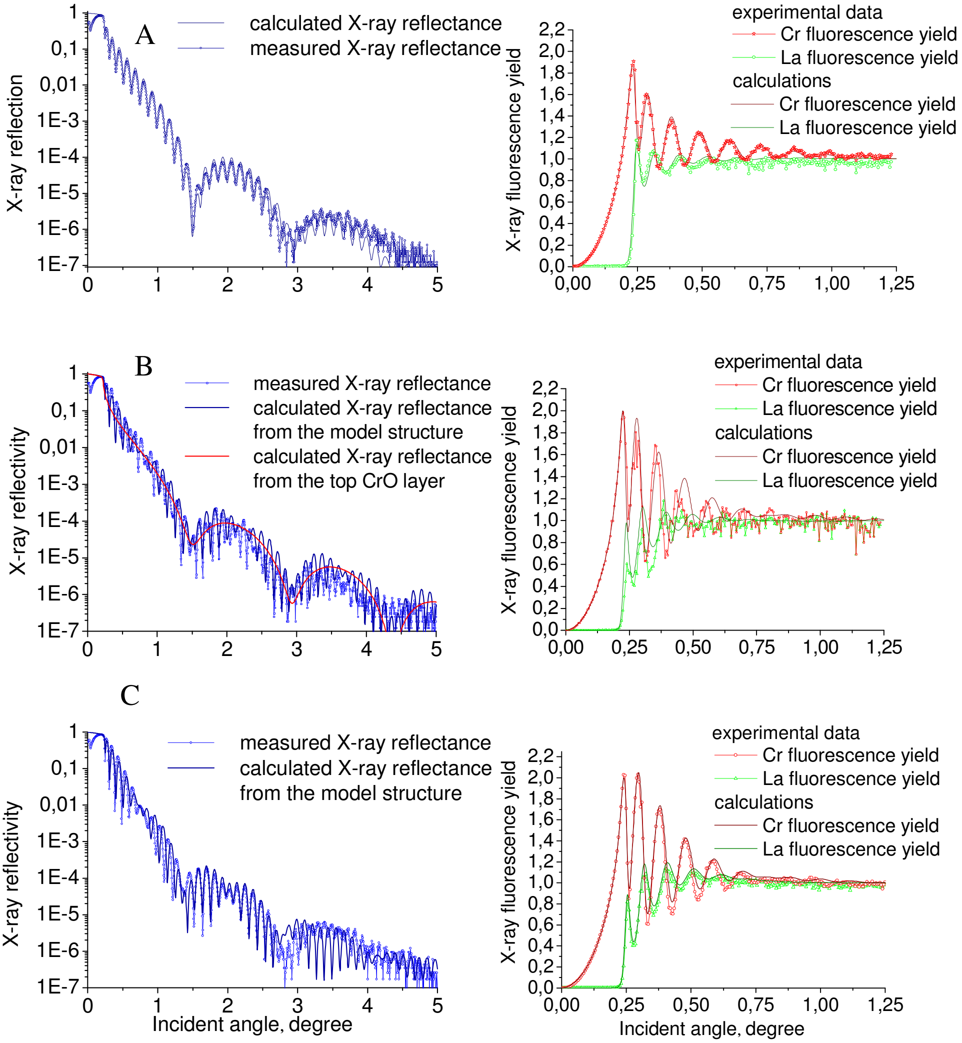

Figure 6.4 Experimental (line + symbol) and calculated (solid line) grazing incidence x-ray reflection (left) and angular dependant X-ray fluorescence (right) curves for samples A, B and C.

The data analysis was performed in two steps. First, the layer thicknesses and approximate densities were obtained by GIXR data analysis. Subsequently, the GIXF data was analyzed using the layered model obtained from the GIXR analysis. Figure 6.3 shows the experimental X-ray fluorescence energy spectrum from sample B, which is similar to all other spectra. The intensities of the La and Cr fluorescence yields are derived using PyMCA [15].

Figure 6.4 shows the results of the combined GIXR/GIXF analysis. Best fit model parameters are presented in table 6.1.

In all samples, the fitted density of Cr was found to be significantly lower than that of bulk Cr (7.19 g/cm^3). Part of the reduced density is explained by increased porosity which is generally observed in ultrathin films deposited by low energy. A further density reduction can be attributed to surface oxidation of the Cr layer, which was observed by XPS.

For sample A, where 2 nm La was deposited, the best results were obtained when assuming a homogeneous layer with density 4.9±0.3 g/cm3. Although these results are actually close to literature references for LaB_6 (4.72 g/cm^3), a slightly increased density could still be explained by the presence of a La-enriched centre region of the LaB_6 layer.

Sample	Cr layer thickness, nm	Cr layer density, g/cm^3	First B_4C thickness, nm	First B_4C density, g/cm^3	Studied layer thickness, nm	Studied layer density, g/cm^3	Second B_4C thickness, nm	Second B_4C density, g/cm^3
A	3.04± 0.05	6.2	31.5± 0.5	2.5	3 ± 0.5	4.9± 0.3	10	2.5
B	3.1± 0.05	6.1	31.5± 0.2	2.5	6 ± 0.5	5.5± 0.6	10	2.5
C	3.2± 0.05	6.5	30.8± 0.5	2.5	6 ± 0.5	6.5± 0.3	10	2.5

***Table 6.1** Obtained structural parameters for fit models (see text for details).*

For sample B, where 6 nm La was deposited, it appeared more challenging to obtain a high-quality fit between GIXR and GIXF simulations and experiments, using a single density for the entire 6 nm layer. This can be explained by the large interaction between B_4C and La, suggesting that the addition of LaB_6 interfaces may improve the quality of the fit. However, fit of the low frequency envelope (red line GIXR plot for sample B, Figure 6.4) and Kiessig fringes still provides the most critical information for determining the GIXF parameters, i.e. thickness of the Cr marker layer and thickness of the first B_4C spacer. The thicknesses of the second B_4C spacer and the La layer do not significantly influence the GIXF angular dependence at low incidence angles and was therefore kept constant during experimental data fit. Thus study of interface parameters were not the goal of this research a satisfactory fit was obtained for model without interlayers with effective La layer density 5.5 ± 0.6 g/cm^3 which is reduced comparable to bulk La density (6.13 g/cm^3) due to LaB_6 compound formation in the interfaces.

Finally, we consider the case for 6 nm La, treated with N ions, labeled as sample C. In contrast to the difficulties observed in the case of 6 nm La (sample B), the GIXRR and GIXRF curves for sample C could be accurately reproduced by model simulations. This result suggests that the La layer can be treated as one layer with a constant density, without strong interaction with the B_4C layers leading to LaB_6 interlayers. The density obtained was 6.5± 0.3 g/cm^3, close to the reported literature value for bulk LaN.

6.4 Conclusions

We have shown that information about ultrathin film densities can be obtained using the Grazing Incidence-X-ray Standing Wave technique (GI-XSW). The sample design described allows one to study ultrathin layers from reactive materials, notably in an application-relevant thin-film state. The obtained densities are in good agreement with current knowledge of interface chemistry in La/B_4C and LaN/B_4C systems. The formation of a LaB_6 compound at the layer interface explains the observed reduction of the density of a 2 nm La layer to 4.9±0.3 g/cm^3, approximately corresponding to the bulk value of LaB_6. Similarly, the obtained density of a 6 nm La layer of 5.5 ± 0.6 g/cm^3 is explained, and compared to the bulk value for La (6.13 g/cm3). The obtained density for LaN is close to the bulk LaN value due to homogeneous LaN compound formation. These results are relevant for the analysis of hard X-ray grazing incidence reflectivity and normal incidence 6.7 nm reflectance analysis, in which cases the known densities are inaccurate to sufficiently fit measured data.

6.5 References

1. Spiller, E., *Soft X-ray Optics*. 1994: SPIE optical Engineering press.
2. Andreev, S.S., et al., *Multilayered mirrors based on La/B4C(B9C) for X-ray range near anomalous dispersion of boron (lambda approximate to 6.7 nm).* Nuclear Instruments & Methods in Physics Research Section a-Accelerators Spectrometers Detectors and Associated Equipment, 2009. **603**(1-2): p. 80-82.
3. Tsarfati, T., et al., *Nitridation and contrast of* B_4C/La *interfaces and multilayers.* Thin Solid Films, 2010. **doi: 10.1016/j.tsf.2010.04.088**.
4. Haussler, D., et al., Quantitative TEM characterizations of La/B4C and Mo/B4C ultrathin multilayer gratings by the geometric phase method. Microelectronic Engineering, 2007. **84**(3): p. 454-459.
5. Tsarfati, T., et al., Reflective multilayer optics for 6.7 nm wavelength radiation sources and next generation lithography. Thin Solid Films, 2009. **518**(5): p. 1365-1368.
6. Andre, J.M., et al., La/B4C small period multilayer interferential mirror for the analysis of boron. X-Ray Spectrometry, 2005. **34**(3): p. 203-206.
7. Gibaud, A., G. Vignaud, and S.K. Sinha, *The correction of geometrical factors in the analysis of x-ray reflectivity.* Acta Crystallographica Section A, 1993. **49**: p. 642-648.
8. Windover, D., et al., Energy-dispersive, x-ray reflectivity density measurements of porous SiO2 xerogels. Applied Physics Letters, 2000. **76**(2): p. 158-160.
9. Wallace, W.E. and W.L. Wu, A novel method for determining thin film density by energy-dispersive x-ray reflectivity. Applied Physics Letters 1995. **67**(9).
10. Zheludeva, S.I., et al., *X-ray standing waves in X-ray specular reflection and fluorescence study of nano-films.* Journal of Applied Crystallography, 1997. **30**(2): p. 833-838.
11. de Boer, D.K.G., Glancing-incidence x-ray fluorescence of layered materials. Physical Review B, 1991. **44**(2).
12. Pelka, J.B., et al., Application of resonance-enhanced X-ray standing waves to the study of layered structures by grazing-incidence X-ray reflectometry and secondary radiation. Journal of Alloys and Compounds, 1999. **286**(1-2): p. 313-321.
13. http://www-cxro.lbl.gov, *CXRO X-ray database*.
14. Yakshin, A.E., et al., Enhanced reflectance of interface engineered Mo/Si multilayers produced by thermal particle deposition. Proc. of SPIE 2007. **6517**.
15. *PyMca*, http://pymca.sourceforge.net/.

7 Model independent X-ray standing wave analysis of periodic multilayer structures

We present a model independent approach for the reconstruction of the atomic concentration profile in a nanoscale layered structure, as measured using the X-ray fluorescence yield modulated by an X-ray standing wave (XSW). The approach is based on the direct regularized solution of the system of linear equations that characterizes the fluorescence yield. The suggested technique was optimized for, but not limited to, the analysis of periodic layered structures where the XSW is formed under Bragg conditions.

The developed approach was applied to the reconstruction of the atomic concentration profiles for LaN/BN multilayers with 50 periods of 35 Å thick layers. Since the estimated thickness of the interface region between the constituent materials is comparable to the individual layer thicknesses, traditional grazing incidence X-ray reflectivity analysis is complicated and not unique. However, using the XSW technique it was possible to reconstruct the La atomic profile despite the large interface thickness, showing that the La atoms are localized within the LaN layers and interfaces and that they do not diffuse into the BN layer. The atomic distributions were found with an accuracy of 1 Å. The analysis of the Kr fluorescence yield showed that Kr atoms originating from the sputter gas are trapped in both the LaN-on-BN and the BN-on-LaN interfaces.

7.1 Introduction

The X-ray standing wave (XSW) technique[1, 2] is applied to non-destructively reconstruct the atomic profiles in crystals and in periodic [3, 4], [5], [6], [7] or aperiodic stratified structures[3, 4, 8-10]. The technique is based on the measurement and analysis of the characteristic signal, for example of the X-ray fluorescence yield, from specific atoms excited by the XSW formed inside a structure. The position of nodes and antinodes of the XSW formed at Bragg reflection conditions in a periodic layered structure or at total external reflection conditions in a non-periodic structure can be modified by changing the incidence angle. The angular dependent intensity of e.g. the X-ray fluorescence yield from the atoms excited by the XSW is now determined by the overlap between the atomic profile and the electromagnetic field. Knowing the electromagnetic field distribution inside the structure, the atomic distribution can be reconstructed from the measured angular dependent fluorescence yield.

In this paper we consider the XSW analysis using X-ray fluorescence. The ideal approach to the atomic profile reconstruction is a simultaneous fit of grazing incidence X-ray reflectivity (GIXR) and XSW data having the atomic profile as a fit parameter. However, this approach is time consuming because of the large amount of fit parameters, and moreover, the outcome may be dependent on the initial model. The complicated data analysis is generally the limiting factor for the application of the XSW technique.

Recently, a model independent approach to the reconstruction of the atomic distribution profile from XSW data was suggested by Cheng et.al. [11] and later extended by Kohli et. al. [12]. The work [11] presents the Fourier transformation of measured fluorescence yields excited by the Bragg-XSW measured from a single crystalline sample. The Fourier transformation requires the measurement of the angular dependent fluorescence yield at different Bragg reflection orders and therefore requires a highly ordered structure. An extension of the Fourier reconstruction based approach for the analysis of thin film structures with long period XSW was presented by Kohli et.al. [12]. This method requires the XSW data to have a large number of fluorescence yield oscillations, and imposes strict requirements on the design of the sample to be analyzed. In the current paper, we present a new approach for a model independent analysis of the XSW data that is based on the direct solution of the ill-defined system of linear equations describing the angular dependent fluorescence yield using the Tichonov regularization technique [13]. Similarly to [12], the presented analysis requires the knowledge of the electromagnetic (EM) field that can be obtained from the analysis of grazing incidence X-ray reflectivity data [14].

The XSW technique is an especially powerful analytical tool when applied to a complex layered structure such as a periodic multilayer. In this paper we will use XSW to analyze the atomic concentration profiles of La and pollutant (Kr) atoms in short period LaN/BN multilayer mirrors. Such multilayers are considered as reflective optical coatings for a next generation EUV lithography[15, 16] at 6.7 nm wavelength and their optical performance is intrinsically linked to the in-depth atomic profiles. The preliminary structural analysis of La/B-based multilayer stacks (La/B and La/B_4C) shows high interface imperfections because of the intermixing between the La and B layers [15]. The passivation of La with N ions improves the quality of multilayer mirror[17]. It can be expected that passivation of both layers has the potential to create diffusion free multilayers because of the chemical stability of LaN and BN.

Especially small fluctuations in the atomic profiles pose a challenge to traditional analysis techniques such as transmission electron microscopy and X-ray reflectometry and we will show that the XSW technique has a unique capability to resolve these details. In this paper, the XSW technique was mainly applied to study the penetration of La into BN layers in LaN/BN multilayers. Additionally the XSW technique was applied to analyze the distribution of the contamination inside the multilayer period.

7.2 Modeling

7.2.1 XSW data analysis

The intensity of the fluorescence yield of atoms in a film is determined by the electromagnetic field $|E(\theta,z)|^2$, depending on the incidence angle θ and distance z from the film surface, and the atomic distribution profile $\boldsymbol{P}$ in the film. For calculations of the EM field it is necessary to divide the entire film into very thin sub-layers where the thickness of individual sub-layers is much smaller than the thickness of the layers, with each sublayer having a constant atomic concentration. In the dipole approximation the angular dependence of the fluorescence yield intensity $Y(\theta)$ is calculated as the sum over all sublayers of the products of the electromagnetic field distributions $|E(\theta,z_j)|^2$ and the concentration of fluorescent atoms in each sub-layer P_j, corrected for the geometrical factor $G(\theta)$ and for absorption of the fluorescence radiation:

$$Y(\theta) = G(\theta)\sum_j P_j \, |E(\theta, z_j)|^2 e^{-\mu_f z_f} \tag{7.1}$$

Here μ_f is the averaged linear absorption coefficient at the fluorescence wavelength on the exit path from the film. The geometrical factor takes into account the variation of the beam footprint with the change of the incidence angle.

If the studied sample is considered to be a periodic multilayer structure that contains N bi-layers with thickness Λ, the atomic profile $\boldsymbol{P}$ will have N identical periods. Assuming a perfect periodicity, the multilayer can be presented as one "effective" period where the electromagnetic field distribution is the summed EM field from all periods in the multilayer. The effective EM field that excites fluorescence for the whole multilayer can now be represented as

$$\bar{I}_j(\theta) = G(\theta)\sum_{k=1}^{N}\left|E(\theta, z_{jk})\right|^2 e^{-\mu_f z_{jk}}, \tag{7.2}$$

where $z_{jk} = D[k-1+(j-1/2)/m]$, $j = [1...m]$ is the number of the sub-layer within one period, m is the number of sublayers in one period and $k = [1...N]$ is the number of the period in the multilayer. Formula 1 can then be simplified to

$$Y(\theta_i) = \sum_{j=1}^{m} P'_j \, \bar{I}_j(\theta_i) \; . \tag{7.3}$$

In formula 7.3, P' is then representative for the atomic distribution along a period. For brevity, the apostrophe will further be omitted.

Having measured the fluorescence angular dependency Y_{exp}, according to the method of least squares the unknown profile P_j is found by minimizing the function

$$\chi^2 = \frac{1}{n-m}\sum_i \frac{1}{\sigma_i^2}\left(Y_{\exp}(\theta_i) - P_j \bar{I}_j(\theta_i)\right)^2 , \tag{7.4}$$

where n is the number of measured angular points and σ_i the statistical error of the fluorescence yield measurements.

Generally, χ^2 can be minimized using a fit procedure if there is no algebraic solution possible. However in the case presented here, the problem can be solved by solving the system of linear equations

$$\partial\chi^2 / \partial P_j = 0 \; . \tag{7.5}$$

After taking the derivative of χ^2, Eq. 7.5 is transformed into [18]

$$\hat{A}\mathbf{P} = \mathbf{b}\,, \tag{7.6}$$

where

$$\hat{A}_{jl} = \sum_{i=1}^{n} \frac{\bar{I}_j(\theta_i)\bar{I}_l(\theta_i)}{\sigma_i^2}\,, \tag{7.7}$$

$$b_l = \sum_{i=1}^{n} \frac{Y_{\exp}(\theta_i)\bar{I}_l(\theta_i)}{\sigma_i^2}\,, \tag{7.8}$$

and $j,l = [1...m]$, the number of the sublayer in a multilayer period.

The system of equations (7.6) can easily be solved numerically for ***P***. However, due to systematic and statistical experimental errors the reconstructed atomic depth profile may exhibit non-physical features such as negative values and strong fluctuations. This effect is the consequence of an ill-posed problem [13]. In order to obtain reasonable solutions, a regularization is introduced in the solving algorithm. The limitation can e.g. be that the profile should be smooth. Mathematically this requirement can be introduced by adding the auxiliary term u in the function χ^2. We use the following auxiliary term:

$$u = \lambda\left[\sum_{j=2}^{m-1}(2P_j - P_{j-1} - P_{j+1})^2 + (2P_1 - P_m - P_2)^2 + (2P_m - P_{m-1} - P_1)^2\right], \tag{7.9}$$

wherein the first term defines the smoothness of the profile amplitude within a period. The second and third terms define continuity on the upper and lower interface, respectively. The smoothening coefficient λ determines the maximum "allowed" changes from P_j to P_{j+1} and should be selected for each separate case individually. The system of equations (7.6) is then transformed into the system of linear equations

$$(\hat{A} + \lambda\hat{D})\mathbf{P} = \mathbf{b}\,. \tag{7.10}$$

Here $\hat{D}$ is the regularization Gram matrix:

$$\hat{D} = \begin{pmatrix} 2 & -1 & 0 & \cdots & -1 \\ -1 & 2 & -1 & & 0 \\ \vdots & \ddots & \ddots & \ddots & \vdots \\ 0 & & -1 & 2 & -1 \\ -1 & \cdots & 0 & -1 & 2 \end{pmatrix}, \tag{7.11}$$

The used Gram matrix is adapted for the periodical structure of multilayer mirrors. A similar type of regularization, although for non-periodic structures, has been successfully applied for the similar problem of reconstructing scatter density profiles from X-ray reflectometry [19].

Although the obtained atomic concentration profile will be smooth, it may still show negative (non-physical) values. The layers with negative atomic concentrations should then be removed by sequential "removal" of the individual equations that correspond to the sub-layers with the largest negative concentrations, followed by searching for a new solution of a lower-rank system of equations.

Unfortunately the suggested approach (Eq. 7.10) does not allow evaluation of errors in the reconstructed profiles because the shape of the reconstructed profile is dependent on the smoothening parameter λ, which influences errors. To estimate errors and the stability of the profile determination, the XSW data can be fitted using a Gaussian shape of the atomic concentration distribution. Errors can be derived from this fit. The fit requires the input of initial parameters for the Gaussian model where the exact positions of a distribution centre are the most important model parameters. These positions can be found by the iterative removal of sub-layers with negative values in atomic concentrations obtained from the solution of the non regularized system of linear equations (7.6).

The methods and procedures described here will be illustrated in the experimental section of the chapter Using the described algorithms the XSW data can be analyzed without any pre-assumptions about the atomic distribution.

7.2.2 Calculation of the EM field

The electron density profile of the periodic multilayer structure was reconstructed by iterative fitting of model-based reflectivity calculations to the measured GIXR data. In the simplest case a layer in a multilayer film can be descried with 4 parameters: layer thickness, interface thickness, layer density and a material composition. The changes in the electron density profile at the interfaces are described by dividing the interface region in equal sub-layers with a thickness of less than 1 Å and assuming a linear transition in the electron density between neighbouring layers. In this model each interface will still be described with one parameter: the thickness of the region of linear transition. A more complex parameterized description of the electron density profile in the interface transition regions could be used, but goes beyond the scope of this work. This description of interfaces as presented here is preferred over the standard Debye Waller or Nevot-Cross approaches when the calculation of the EM fields in the interface regions is required.

The reflectivity calculations were performed using the Abeles matrix formalism[20] which requires the multiplication of the characteristic matrices that describe electromagnetic wave penetration through all the layers in the sample, including the sub-layers in the interface regions. If the multilayer has good periodicity the and periods can be assumed identical, the Chebishev polynomials can be used [21] to calculate analytically the N^{th} power of the characteristic matrix for each period in the multilayer. This limits the number of matrix multiplications to the calculation of the characteristic matrix for one period only. This approach can be applied if the errors introduced in the parameter determination by aperiodicity of the multilayer are within the general uncertainty of parameter determination.

7.3 Experimental

The GIXR data were measured using a PANalytical X'Pert PRO diffractometer using $CuK_{\alpha1}$ radiation and a 4xGe(220) asymmetrically cut monochromator. The measurements were done using a constant 2θ step of 0.005 degrees and 2 seconds of exposure at each step. The XSW measurements were performed at the Hasylab E2 beamline of the DESY synchrotron radiation facility. The bending magnet radiation was monochromized for the wavelength of 0.71 Å. The fluorescence spectra were measured for 5 seconds per angular step using a Roentec energy dispersive detector. Angular scans were repeated in a fixed range of angles around the first Bragg reflection peak and the signals were summed until the statistical error of the accumulated integral fluorescence yield was better than 1%.

The 50 period LaN/BN multilayer structure was deposited using DC magnetron sputtering of La and B_4C targets using Kr as a sputter gas. This number of period was selected as a compromise between the number of periods required for the formation of the contrast X-ray standing wave, the excitation of sufficiently intense fluorescence radiation and the stability of the deposition process. The passivation of La and B_4C layers was done using low energy N-ion treatment of the deposited layers [22]. XPS measurements were used to optimize the parameters of metrication for the deposition of LaN and BN films (optimization is not presented here). The ratio of La layer to period thickness was selected 0.4 for optimal optical performance.

7.4 Results

7.4.1 Electron density profile reconstruction

The electron density profile was reconstructed from the fit of the GIXR data in order to calculate the EM field for XSW analysis. The analysis of GIXR data was performed in two steps: first the fit was performed with a model that describes a 50 times repeated structure, the multilayer period, varying the period structure parameters (layer and interface thicknesses and densities), and assuming no period variation along the stack. Separately, a second fit was performed where the parameters of all periods were varied individually. From the first fit the average period structural parameters and their statistical errors were obtained. From the second fit the individual parameters of all layers were obtained and their deviation from the average was determined. Comparing both the averaged and individual parameter sets allows checking the applicability of the model with identical periods for the XSW analysis.

The average values were obtained for the model containing 49 identical periods. The parameters of the top layers were fitted separately assuming that contact with ambient gases possibly changes the top layer structure. The best model representation of the electron density profile is shown in Figure 7.1 a. As depicted in Figure 7.1 a, each interface consists of two linear segments with different slopes each, indicating that one simple linear transition is not good enough. For each parameter the fit errors were estimated. The parameter values and their errors are shown in table 1 in the column “Average”. The fit goodness of χ^2=2.2 confirms the fit quality.

In the second fit we allowed all 50 periods to have individual layer parameter. This “individual layers” fit improved the fit quality to χ^2=1.12 mostly because of the better match of the Kiessig fringes (Figure 7.2). Analysing the distribution of individual layer parameters, their standard deviation from their average values is determined and presented in table 1 in the column “Deviation”. The obtained period thickness of the multilayer determined from both fits was Λ= 43.4 Å with a standard deviation of the many-period fit s_D = 0.24Å, close to the error in the period determination from the fit of the model with identical periods and small compared to the actual value. This confirms that the model with identical periods describes the density profile in the full stack well and may be used for XSW data analysis. The EM field was finally calculated using the Abeles matrix formalism for the reconstructed averaged multilayer profile and summed along the z direction over all periods according to Eq. (7.2). Figure 7.1b shows the averaged EM field visualizing positions of the nodes and antinodes of the XSW within a period.

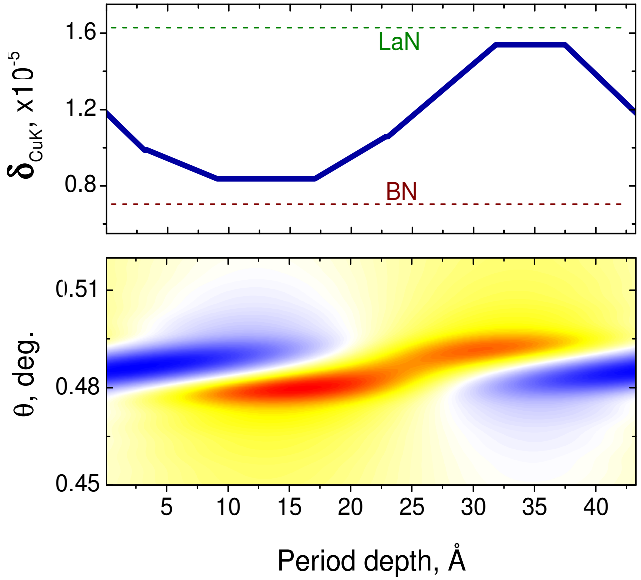

Figure 7.1 Reconstructed electron density profile in the LaN/BN multilayer (a) and EM field distribution in the vicinity of the 1-st Bragg peak (b) calculated for the wavelength of 0.71 Å used in the fluorescence yield measurements.

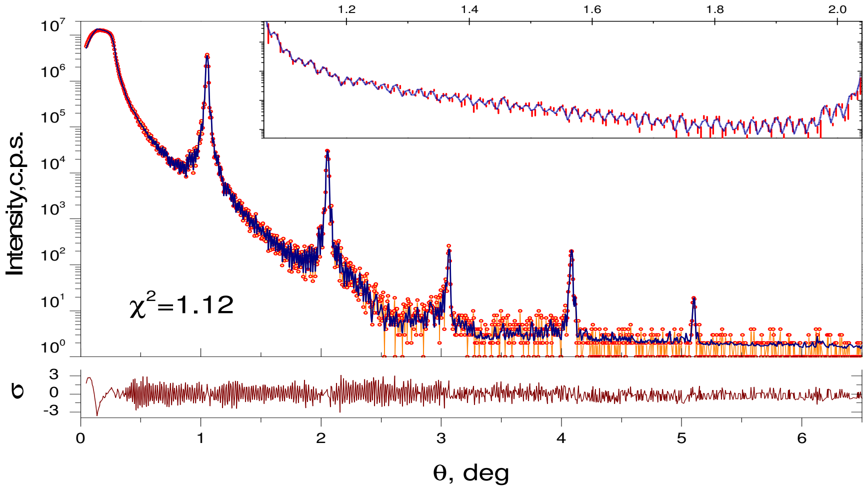

Figure 7.2 Experimental and simulated GIXR data for the model with individually defined periods. The insert shows the measured and simulated Kiessig fringes between first and second order Bragg peaks.

From the GIXR profile it is observed that approximately 70% of the period thickness is in the interface state (referring to the two gradients in between the LaN and BN). This would suggest that there is significant intermixing in the multilayer.

	Layer thickness, Å		The interface transition layer thickness, Å		Density, g/cm^3	
	Average	Deviation	Average	Deviation	Average	Deviation
BN	7.95±0.16	0.19	14.9±0.2	0.2	2.7 ± 0.05	0.1
LaN	5.63±0.08	0.21	14.8±0.2	0.3	5.8 ± 0.1	0.13

Table 7.1 LaN/BN model parameters reconstructed from GIXR. For each parameter we show averages over all the periods and a standard deviation of the values for all 50 periods.

7.4.2 Atomic distribution profile reconstruction

A typical measured fluorescence spectrum is presented in Figure 7.3. Additional to the expected La L fluorescence yield, fluorescence from Si (substrate) and Kr was detected. Kr was used as the magnetron sputtering gas, and its presence indicates trapping of Kr in the multilayer. The small doublet at 3 keV originates from the Ar Kα and β lines. The intensity of this signal corresponds to the intensity of Ar from the ambient environment. For XSW analysis, the background corrected integral intensity of La L and Kr K fluorescence radiations were determined at a range of angles of incidence around the first order Bragg reflection.

The angular dependencies of the Kr and La fluorescence yields calculated based on the direct solution of the system of linear equations 6, using EM fields reconstructed from the GIXR measurements, are presented in Figure 7.4. The corresponding reconstructed La and Kr atomic density profiles are presented in Figures 5a and 5b. Note that all atomic density profiles presented in Figure 7.5 are normalized such that the integral of the profile is unity, corresponding to the probability density of the atom distribution in the period of the multilayer structure. Although a very good agreement between simulations and experiments is observed in Fig 7.4, the reconstructed atomic profiles are clearly non physical when no limitations are introduced in the profile, as can be observed from the negative probabilities in Figs. 7.5 a and 7.5 b. Note that even for a non physical solution the fit goodness for La (χ^2=2.97) and for Kr (χ^2=3.29) are not equal to unity because of the presence of systematic errors in the measurements. For other solutions we will not present the calculated curves but will indicate the values for the obtained χ^2 that need to be compared with the values obtained for a non regularized solution.

To resolve the ill-posed problem, limitations to atomic profiles were introduced according to eq. 7.10. For smoothening of the profile, the coefficient $\lambda=10^{-8}$ was used for both element distributions. This value for λ was selected to provide the best fit of the measured to calculated XSW data. The fit quality for smoothed profiles is just slightly worse than for not smoothed profiles: χ^2=6.5 for La and χ^2=4.4 for Kr. The resulting atomic profiles are presented in Figures 7.5 c and 7.5 d. Note that the smooth profile is still physically impossible because of the locally negative density values for both materials. After the sequential removal of negative probability densities and subsequent solving of the reduced system of equations (7.10), the final profiles were found and are shown in Figures 7.5 e and 7.5 f. The fit goodness of the final fit (χ^2=4.6 for La and χ^2=3.1 for Kr) is actually better than that for the initial smoothed profile that allowed negative probability densities because of the reduced degrees of freedom during the calculations of the χ^2 function.

To determine the accuracy and stability of the reconstructed profiles, additional analysis was performed. Starting from the non-smoothened profiles (Figures. 7.5 a and 7.5 b), sub-layers with the most negative value were iteratively removed until no negative values remained, resulting in the profiles shown in Figs. 7.5 g and 7.5 h. The obtained profiles correspond to the peak positions of La distribution profiles. The thus determined profiles were further resolved by the fit of model based calculations of fluorescence yield to measured XSW data, assuming that concentration profiles follow a Gaussian distribution form with peak centre position and peak width as fit parameters. The centre positions of the initial Gauss profiles were obtained from Figures 7.5 g and 7.5 h. Because of the relative importance of the single peak at z=35 Å, a single Gaussian distribution at this position was used for the analysis of the La profile. The result of the reconstruction is presented in Figure 7.5 i. The fluorescence yield of Kr was simulated with two separate Gaussians located at the positions obtained from Figure 7.5 h. Comparing the La profiles from Figures 7.5 e and 7.5 h we can conclude that all exhibit the same location of La within the period, within a 1 Å accuracy. The same conclusion can be drawn for Kr.

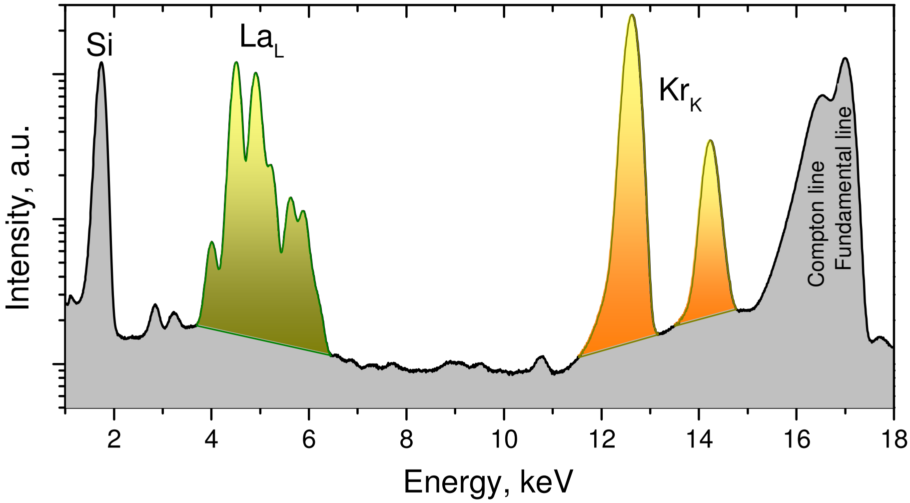

Figure 7.3 Typical X-ray fluorescence spectrum measured from the LaN/BN multilayer.

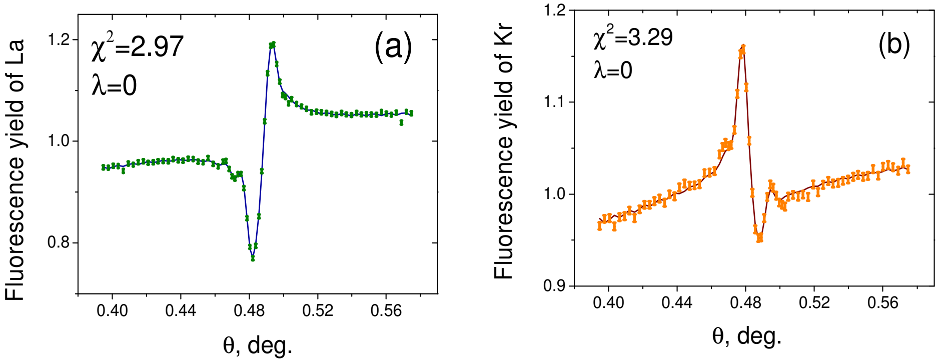

Figure 7.4 Experimental (symbols) and simulated (solid lines) X-ray fluorescence yields for La (a) and for Kr (b) in the region of the first Bragg peak region.

7.5 Discussion

The model-independent technique for XSW data analysis presented here expands the series of model independent approaches presented in works [11] and [12] and completes the set of model independent approaches for all types of XSW techniques: Bragg-XSW for single crystals, long period XSW for layered structures and Bragg XSW for periodic multilayer structures.

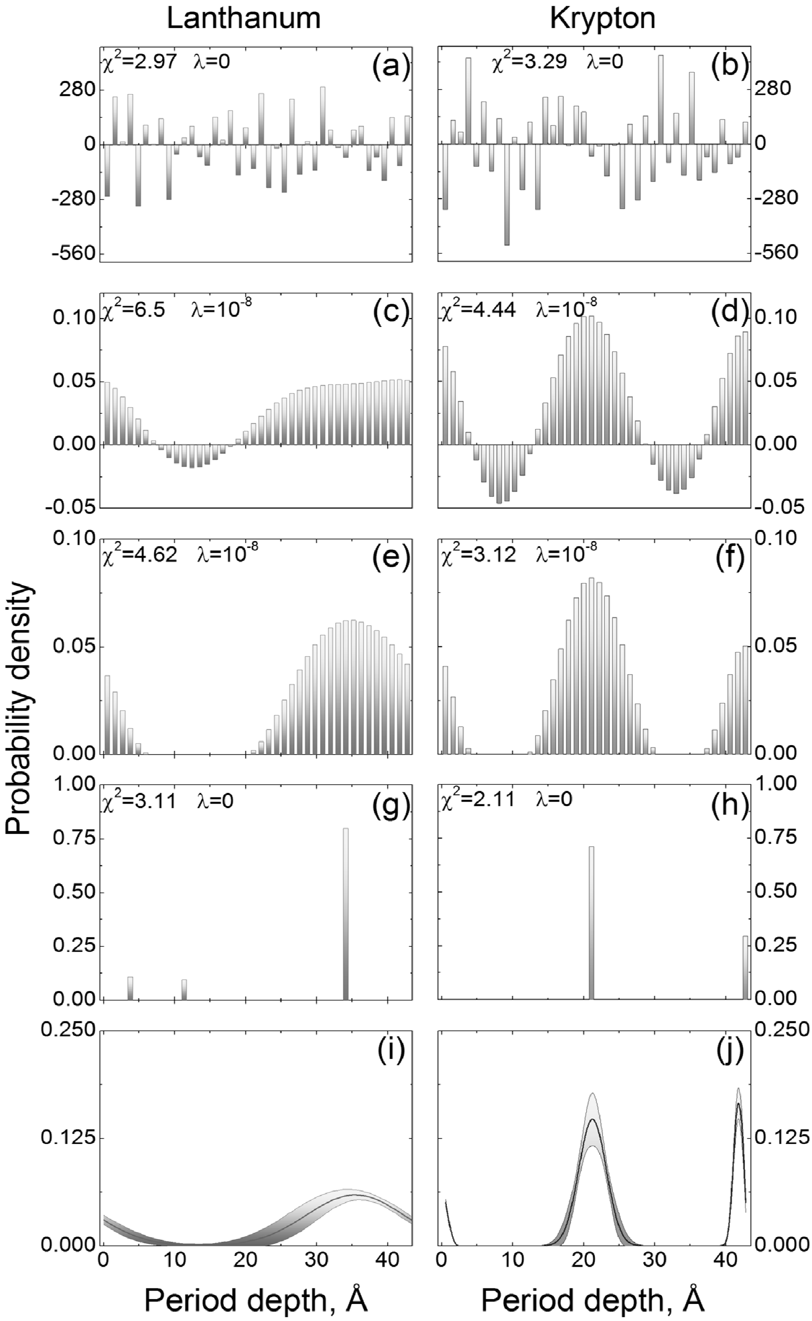

Figure 7.5 Reconstructed atomic profiles for La and Kr using no profile limitations (a and b), profile smoothening (c and d), and smoothening with iterative removal of sublayers with negative values (e and f). Also shown are non-smoothened profiles with iterative removal of sublayers with negative values (g and h) and profiles obtained using Gaussian atomic distributions (i and j).

The benefits of the current approach is that for the reconstruction of atomic profiles by direct solution of Equation (7.10) the XSW data can be measured only for one order of Bragg reflection. The disadvantage is that regularization procedure forces the profile to be smoothed and inaccurate selection of the smoothening coefficient λ may force a too much smoothened profile. Taking into account that in Equation (7.6) the fluorescence yield is excited by the general EM field shape, the current approach can be extended to the long-period XSW technique. However there the modification of the regularization technique might be required.

The analysis of errors in the profiles reconstructed using the XSW technique shows that the position of the maximum in the atomic distribution profile can be determined with an accuracy of 1 Å. The analysis of errors was performed assuming that the EM field does not change with the variation of the atomic profiles, and suggests that the derived error is slightly underestimated. However if all experimental artefacts connected to the beam spectral and geometrical resolution and goniometric uncertainties are taken into account, the reconstructed positions of atom localization are reliable. We should note that because of the shape of the EM field, an increase of the atomic distribution width will lead to a decrease in the accuracy of the shape of the distribution, reducing the accuracy of the profile width determination. We also note that the XSW technique yields the averaged over all periods profile, and a strong aperiodicity in the sample will therefore be misinterpreted as a blurring of the atomic distribution. The GIXR technique applied here for the EM field reconstruction is sensitive to the periodicity of the multilayer and will allow estimation of period fluctuations before the XSW analysis is performed.

Figure 7.6 shows a comparison between the optical contrast profile obtained from GIXR and the atomic distribution profile obtained from the XSW analysis. As discussed in the previous section, the atomic distribution is presented in terms of a normalized probability density per element. In absolute value, the amount of Kr is approximately one order of magnitude less than La. In apparent contrast to the suggestion made based on the GIXR analysis about the intermixing between LaN and BN layers, the XSW analysis shows that La is well localized and the width of the La distribution corresponds to 40% of the period thickness, as expected from the deposition design. The absence of La atoms in the B layer indicates that the metrication of both layers helps to prevent the La-B intermixing in the stack.

The unique result of the XSW analysis is a non destructive analysis of the impurity distribution. A small residue of the sputtering gas Kr could be detected and appears localized in the interface regions. Apparently, Kr neutrals backscattered from the magnetron target (with energies ~300 eV during La sputtering and ~ 600eV during B_4C sputtering) are capable to penetrate through the already deposited layers and be trapped in the interfaces. Kr has a high absorption for the 6.7 nm wavelength and its presence will reduce the reflectance.

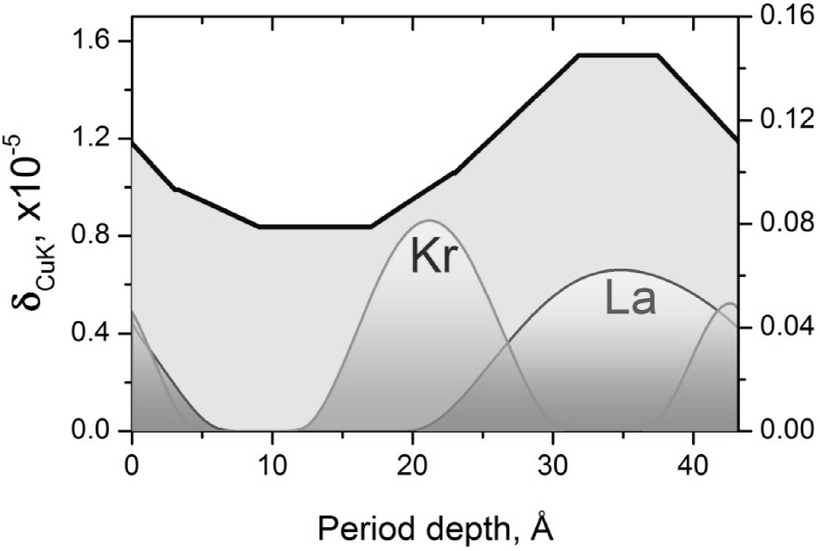

Figure 7.6 Comparison of obtained electron density and atomic profiles.

7.6 Conclusions

As demonstrated in this paper, the analysis of X-ray standing wave data from periodic multilayer structures based on the solution of linear equations describing the fluorescence yield, allows a fast and model independent reconstruction of atomic profiles. The approach was applied to Bragg-XSW data from a LaN/BN multilayer structure. The obtained profile of the La atoms in the structure showed an accurate, 1Å localization of La atoms within the LaN layer and the absence of La atoms in the BN layer. Additionally, the contamination of the multilayer by Kr atoms, trapped during the magnetron deposition process, was revealed. It was found that these Kr atoms are distributed inside the interface regions. The sensitivity of the XSW technique to such atoms remains high, even though their presence does not change the electron density profile. This demonstrates that XSW is capable to provide non-destructive depth resolved elemental composition with sub-nm accuracy.

7.7 References

1. Afanasev, A.M. and V.G. Kohn, Zh.Eksp.Teor.Fiz, 1978. **74**: p. 300.
2. Kovalchuk, M.V. and V.G. Kohn, Usp.Fiz. Nauk 1986. **149**(69).
3. Zegenhagen, J. and A. Kazimirov, *The X-ray Standing Wave Technique: Principles and Applications*: World Scientific Publishing Company Incorporated.
4. Zheludeva, S.I., et al., Thickness and density determination of ultrathin solid films comprising multilayer x-ray mirrors by x-ray reflection and fluorescence study. Review of Scientific Instruments, 1992. **63**(1): p. 1519-1522.
5. Tiwari, M.K., K.J.S. Sawhney, and G.S. Lodha, Characterization of trace embedded impurities in thin multilayer structures using synchrotron X-ray standing waves. Surface and Interface Analysis. **42**(2): p. 110-116.
6. Ghose, S.K. and B.N. Dev, X-ray standing wave and reflectometric characterization of multilayer structures. Physical Review B, 2001. **63**(24): p. 11.
7. Zheludeva, S.I., et al., New method of ultra-thin film characterization applied to the investigation of C/Ni/C structures under heat load. Thin Solid Films, 1995. **259**(2): p. 131-138.
8. Bedzyk, M.J., et al., X-ray standing waves: a molecular yardstick for biological membranes. Science, 1988. **241**(4874): p. 1788-1791.
9. Gupta, A., et al., Depth profiling of marker layers using x-ray waveguide structures. Physical Review B, 2005. **72**(7): p. 075436.
10. Roddatis, V.V., et al., The microstructural and optical properties of Ge/Si heterostructures grown by low-temperature molecular beam epitaxy. Journal of Materials Research. **28**(11): p. 1432-1441.
11. Cheng, L., et al., Fourier-Expansion Solution of Atom Distributions in a Crystal Using X-Ray Standing Waves. Physical Review Letters, 2003. **90**(25): p. 255503.
12. Kohli, V., M.J. Bedzyk, and P. Fenter, Direct method for imaging elemental distribution profiles with long-period x-ray standing waves. Physical Review B. **81**(5): p. 054112.
13. Tikhonov, A.N. and V.I.A. Arsenin, *Solutions of ill-posed problems*. 1977: Winston.
14. Yakunin, S.N., et al., X-ray diagnostics of heterostructures with quantum dots. 2004: p. 573-578.
15. Makhotkin, I.A., et al., *Wavelength selection for multilayer coatings for lithography generation beyond extreme ultraviolet.* Journal of Micro/Nanolithography, MEMS, and MOEMS, 2012. **11**(4): p. 040501-1-040501-3.
16. Platonov, Y., et al., *Multilayers for next generation EUVL at 6.X nm* SPIE, 2011. **8076**(22): p. 1-9.

17. Tsarfati, T., et al., *Nitridation and contrast of B_4C/La interfaces and multilayers.* Thin Solid Films, 2010. **518** p. 7249-7252.
18. Chuev, M.A., et al., Alternative approach for evaluation of Messbauer spectra of nanostructured ferromagnetic alloys within generalized two-level relaxation model. Journal of Experimental and Theoretical Physics Letters, 2002. **76**(9): p. 558-562.
19. Hohage, T., K. Giewekemeyer, and T. Salditt, Iterative reconstruction of a refractive-index profile from x-ray or neutron reflectivity measurements. Physical Review E, 2008. **77**(5): p. 051604.
20. Abeles, F., *La théorie générale des couches minces.* Le Journal de Physique et le Radium, 1950. **11**: p. 307-310.
21. Born, M. and E. Wolf, *Principles of optics*. 1999: Cambridge University Press.
22. Louis, E., et al., Nanometer interface and materials control for multilayer EUV-optical applications. Progress in Surface Science, 2011. **86**(11): p. 255-294.

8 Valorization

The research described in this thesis has been inspired by the perspectives of application of La/B based optics in future lithographic equipment used for IC manufacturing. The development of a new type of multilayer optics from its first design to an industrial product takes a long time. For example, it took more than 15 years to develop the optical coatings for 13.5 nm lithography to their current performance level. The reason is that the research of a new reflective coating, especially in its initial stage, is more or less a “one lane road”. It is difficult to divide it into sub topics that can be investigated in parallel. The exact composition including the development of the thermodynamically stable compounds and possibly diffusion barriers has to be investigated before process optimization can take place. Because of the lengthy research time it is required to have all basic elements such as optics and sources already explored before the starting point of the industrial development project can take place. Therefore, the study described in this thesis, although highly applicable in industry, was carried out in a research environment. Considering this, the Thin Film Nanomanufacturing program of the Dutch Technology Foundation STW was an excellent platform for this type of research.

The lithography industry poses the strictest requirements for the highest possible reflectivity of multilayer optics because the integral reflection from each individual mirror will determine the optical column transmission. The higher transmission of optical column will allow reaching the higher chip production efficiency. For comparison, the reflectivity of Mo/Si multilayer mirrors used in current generation EUV lithography at 13.5 nm is slightly below

70% what is close to theoretical maximum of 75% reflection. It can be expected that for La/B similar reflectivity requirements will be posed.

The physics research on growth, intermixing and layer properties, extensively discussed in thesis, is the basis for the development of multilayer coated optics. An important indicator of the potential for valorization, particularly in lithography systems for semiconductor industry, is the highest achievable reflectance of the mirrors. As a figure of merit of this thesis work, the measured normal incidence reflectance at 6.x nm wavelength is presented in Figure 8.1. Figure 8.1 shows that as the result of technology development during this project the reflectivity of multilayer mirrors for 6.x nm wavelength was increased from 43% to 57% at 6.6 nm, which is the highest reflectance value reported in literature to date, however it is still considerably lower than theoretical value of 80%. As major steps of multilayer development we can indicate the replacement of B4C with pure boron as the spacer material and the gradual optimization of the nitridation of the La layers.

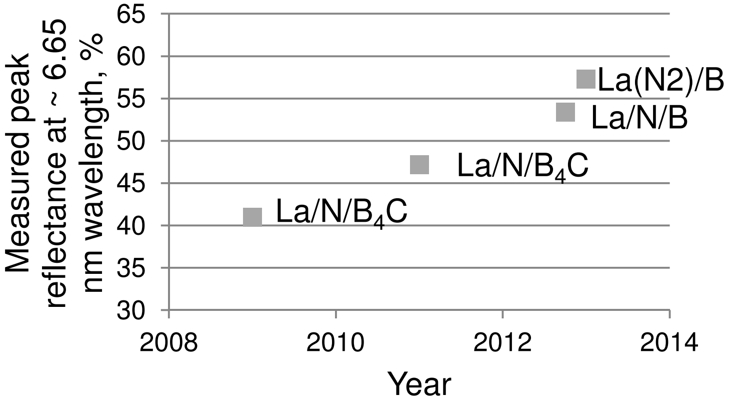

Figure 8.1 The evolution of 6.6 nm reflectivity development at nSI laboratory at FOM DIFFER.

For the lithography industry this research can be seen as basic research of optical coatings - the key element of the optical system. The contact with industry provided essential input for the project. Colleagues from Carl Zeiss SMT and ASML stated several research questions that are on the one hand of practical interest and on the other hand have scientific relevance. Good examples of this type of questions are the requests for analysis of the reflectivity spectra and the optical potential of La/B-based multilayers, as presented in chapters 3 to 5. To answer these questions, an extended experimental assessment of the multilayer reflectivity was required. Firstly, the accuracy of tabulated optical constants was found to be insufficient and secondly the optical properties of ultrathin layers within the multilayer environment were different from the relatively thick layers that are typically used for the measurements of optical constants. For industry this research provided the reflectivity spectra and values that are required for wavelength selection and making a draft estimation of the optical column transmission.

Generally, La/B-based multilayer mirrors can also be interesting for the industry that develops systems for spectroscopic analysis of low Z elements. For this application the most important spectral characteristic of a multilayer is a narrow bandwidth because it determines the spectral resolution of multilayer-based monochromators. For this type of application standard multilayer coatings are typically replaced with multilayer gratings and the research presented in this thesis can serve as the starting point for a LaN/B based multilayer gratings study.

Mirrors for 6.6 nm and longer wavelength can also be used for free electron lasers working in this wavelength range. For FEL application the reflectivity coefficient is not very important because of the large flux of a FEL beam. However, because of this every optic used in a FEL setup will be exposed to a high thermal and radiation load. To be applicable there, the thermal and radiation stability of LaN/B multilayers should be studied.

Extensive research was done in the field of precise X-ray analysis techniques for the characterization of multilayer structures, namely the grazing incidence X-ray reflectivity (GIXR). This GIXR technique is well-known for the determination of the multilayer period thickness. This technique has a capability to analyze the detailed structure of multilayers including interface thicknesses and layer densities. However this requires detailed fitting of the calculated GIXR curve to measured data. There are several commercial programs, developed by the X-ray analytical tools manufacturers as well as free programs like IMD and GenX, designed for the analysis of X-ray reflectivity data. Almost all of them are suitable but not optimised for the analysis of short period multilayer mirrors especially with thick interfaces and large intermixing of layers, like the La/B based mirrors studied in this thesis. The data analysis in non optimized programs take a lot of time (approx, 4-6 hours or longer) limiting the number of samples that can be analysed in detail. We have optimized the traditional approach (see chapter 2 and 7 for details) and developed a flexible MatLab based program for the analysis of grazing incidence X-ray reflectivity data what makes this analysis easier and faster. This can be of great interest for an industry that develops analytical software and equipment.

9 Summary

The physics investigations described in this thesis have been inspired by the perspective of the application of La/B-based multilayer mirrors in photolithography. This perspective however, demands the highest possible reflectance of the mirrors and full control over the multilayer growth process. The corresponding research in this thesis therefore covers the following topics: a theoretical and experimental analysis of the spectral properties of La/B-based multilayer stacks, an experimental layer composition and growth study of the candidate La/B-based multilayer optics, and the development of techniques to enable characterization of the internal structure of such multilayers.

In theory, La/B multilayer mirrors have the potential to reflect up to 80% at a wavelength of 6.64 nm at normal incidence. Yet, the value is denoted as 6.x nm since the lithography community has not standardized to this value due to uncertainties in the light source approach. Also the multilayer development task turned out to be non-trivial: individual layers of approximately 1.5 nm thickness do have interface layers of comparable thickness and a high layer interdiffusion, which limits the multilayer reflectivity. However, the replacement of La with LaN dramatically improved the structural and optical quality of the multilayer. Two ways of nitridation of the La layers have been investigated: treatment of every La layer with N-ions directly upon La deposition, and the deposition of La in a N_2 environment. An optimization showed that both techniques enable the deposition of LaN/B multilayers with comparable reflectivity, albeit that the deposition in N_2 atmosphere leads to a better optical contrast. Applying such nitridation to the La layers and optimization of the deposition process has improved the peak reflectance from below 43 %, the value at the start of this thesis research, up to 57.4 % at normal incidence at 6.6 nm, which is the highest reflectance reported worldwide so far. The gap to the theoretical value is explained by interface imperfections and the degree of diffusion of nitrogen into the boron layers, and several suggestions for further control of the growth mechanisms of LaN/B multilayers are given.

This multilayer optimization requires adequate atomic scale analysis of its internal structure, but the available methods are not suitable when the thickness of the interlayer is comparable to the thickness of the layer itself. Therefore, we developed an X-ray reflection data analysis method based on a rigorous description of the interface layers. To deal with the different sensitivity of X-rays and EUV light for the electron density contrast between La and B, we have combined this X-ray and EUV reflectivity analysis. This combined analysis allowed us to increase the accuracy of the structure reconstruction. To obtain La atomic-specific information of our multilayer mirrors, we have analyzed the X-ray fluorescence yield from the multilayer stack excited by the X-ray standing wave, formed as a result of interference between incident and reflected X-ray beams.

In summary, this thesis provides the pioneering research on reflective multilayer coatings for 6.x nm light providing the first experimental results and assessments of their further perspectives for the next generation EUV photolithography.

9* Абстракт

В данной диссертации представлены результаты исследования структуры и свойств зеркал для жесткого ультрафиолетового излучения 6.7 нм, которые в перспективе могут быть использованы в качестве зеркал для литлграфии следующего поколения. Для обеспечения возможности применения многослойных зеркал, особенно в литографии, необходимо максимально оптимизировать их отражательную способность.

Классические зеркала не подходят для работы с излучением с длиной волны 6.7 нм из-за очень низкого (порядка 0.01%) коэффициента отражения. Для отражения данных длин волн используются периодические многослойные покрытия La/B с толщиной индивидуального слоя в 1.5 нм (0.0015 мкм) и содержащие около 200 пар слоев. Сложность изготовления таких зеркал заключается в том, что ультратонкие слои La и B должны иметь минимальные толщины интерфейсов и наиболее близкие к теоретическим значения плотности, что тяжело достигается при данной толщине слоев. В начале исследования, описанного в данной работе, был продемонстрирован коэффициент отражения в 43% для многослойной структуры LaN/B_4C. Было обнаружено, что пассивация лантана азотом ведет к увеличению отражения многослоек, хотя оптимизация данного процессе не была проведена, так же причины улучшения отражения не были детально проанализированы.

В первую очередь мы провели оптимизацию процесса пассивации лантана азотом, что привело к увеличению коэффициента отражения до 47%. Затем для улучшения оптического контраста было предложено

заменить использованный ранее карбид бора на чистый бор, что сразу же привело к увеличению отражательной способности многослоек до 53%. В дальнейшем мы исследовали различные способы нитридирования лантана, включая использованный ранее способ облучения напыленного слоя лантана ионами азота и реактивное магнетронное напыление лантана в смеси газов аргона и азота. Дальнейшая оптимизация процесса напыления многослойной структуры привела к увеличению отражения до 57%, что на данный момент является самым высоким коэффициентом отражения, измеренным при нормальном падении на длине волны 6.6 нм.

Оптимизация процесса напыления многослойных систем невозможна без детального анализа их структуры. Для анализа зеркал были адаптированы классические методы рентгеновской рефлектометрии, анализа отражения ультрафиолета и стоячих рентгеновских волн. Адаптация была необходима из-за чрезвычайно малой толщины слоев в образцах и сильного перемешивания между слоями.

Таким образом, в данной диссертации представлены исследования многослойных покрытий для излучения с длиной волны 6.x нм. Продемонстрированы первые экспериментальные результаты и оценки их дальнейших перспектив использования в EUV фотолитографии следующего поколения.

9** Samenvatting

Het natuurkundig onderzoek gepresenteerd in dit proefschrift is geinspireerd door de potentiele toepassing van La/B multilaag spiegels in photolithografie. Deze applicatie vereist een zo hoog mogelijke reflectie van de spiegels en volledige controle over het groeiproces van de multilagen. Het onderzoek beslaat om die redenen de volgende onderwerpen: een theoretische en experimentele analyse van de spectrale eigenschappen van op La/B gebaseerde multilagen, een experimentele analyse van de chemische samenstelling en groei van op La/B gebaseerde multilaagen en de ontwikkeling van analysetechnieken om de interne structuur van zulke multilagen te karakteriseren.

In theorie hebben La/B multilaag spiegels de potentie om een reflectie van 80% te behalen voor licht van 6.64 nm onder een rechte hoek van inval met het oppervlak. In de lithografiegemeenschap wordt de waarde van de golflengte echter vaak als 6.x nm genoteerd, omdat de precieze waarde die uiteindelijk gebruikt zal gaan worden nog niet bekend is, mede door onzekerheden omtrent de lichtbron. Maar ook de ontwikkeling van de multilagen is niet triviaal gebleken: de lagen in de multilaag hebben een dikte van ongeveer 1.5 nm, vormen interlagen met vergelijkbare dikte en vertonen een hoge mate van diffusie met naburige lagen, eigenschappen die de reflectiviteit van de multilaag beïnvloeden. De vervanging van La door LaN heeft een significante verbetering van de structurele en optische kwaliteit van de multilagen opgeleverd. Er zijn twee methoden onderzocht om LaN lagen te produceren: behandeling van La lagen met stikstofionen tijdens depositie en het opdampen van La in een atmosfeer van stikstof gas. Een optimalizatiestudie heeft aangetoond dat beide technieken depositie van LaN/B multilagen mogelijk maken met vergelijkbare reflectiviteit, hoewel de laatstgenoemde methode tot een beter optisch contrast tussen de LaN en B lagen leidt. Het toepassen van stikstof in het opdampen van La lagen alsmede verbeteringen in het algehele depositieproces hebben geleid tot een verbetering van de reflectie van 43%, de record waarde aan het begin van dit werk, naar 57.4% onder normale hoek van inval bij een golflengte van 6.6 nm, wat wereldwijd de hoogst gerapporteerde waarde is tot nu toe. Het verschil met de theoretisch maximaal haalbare waarde valt te verklaren door imperfecties in de grensvlakken en diffusie van stikstof in de boor lagen. In het werk worden verscheidene suggesties gegeven om het groeiproces van LaN/B multilagen verder te kunnen controleren en beheersen.

De multilaagoptimalizatie in dit werk vereist een adequate analyse van de interne structuur op atomaire schaal, maar bestaande technieken zijn niet toepasbaar op multilagen met een vergelijkbare dikte van lagen en interlagen. Om die reden hebben we een X-ray reflectie data-analysemethode ontworpen, gebaseerd op een gedetailleerde beschrijving van de interlaag. Om de verschillende gevoeligheden van Röntgen- en EUV straling voor het verschil in elektronendichtheid in La en B te benutten hebben we deze Röntgenanalyse met de EUV-reflectiviteitsanalyse gecombineerd. We hebben de X-ray fluorescentie van de multilagen geanalyseerd om Lanthaan specifieke informatie te verkrijgen.

Samenvattend beschrijft dit werk het pionierende onderzoek naar reflectieve multilagen voor 6.x nm, biedt de eerste experimentele resultaten en een uiteenzetting betreffende de vooruitzichten van de toepassing van LaN/B multilagen voor een eventuele volgende generatie EUV photolithografie.

10 Acknowledgements

First of all, I would like to thank my supervisors, Fred and Eric, for giving me the opportunity to carry out the current research, guiding me and, at the same time, providing me with the for a scientist necessary freedom in selecting the research path. Especially, I would like to thank you for supporting my conference visits and external experimental trips. This allowed me to extend my network and enrich the research with interesting experiments.

I am grateful to my daily supervisor Erwin for his critical approach that helps to plan experiments carefully, for his patience during the correction of the first drafts of the articles, and last but not least, for his XPS measurements and analysis that he did for this research. This analysis was not introduced in detail in my thesis but generally it contributed greatly to the La/B multilayer research.

I would like to thank my friend and colleague Sergey Yakunin, who worked with me on the X-ray analysis of the multilayer, for his enormous support and very constructive critics. Here I also would like to thank Robbert for his interest and collaboration in the field of X-ray anal***ysis*** techniques.

I would also like to thank my friend Alexey from MEPhI for introducing me to the FOM project, where I started to work as a PhD student. I would like to thank Saskia for giving me a lot of help when I just came to the Netherlands. Especially, I would like to acknowledge Noortje Khan and the institute manager Wim Koppers for their help with the difficult housing situation during my first year in the Netherlands.

I would like to thank our colleague at DESY, Dmitry Novikov, for his support of the XSW experiments and providing us the time at the E2 beamline on DORIS. I am grateful to Peter Siffalovic and Eva Majkova for providing me the time for GISAXS experiments during their measurements in DESY. Many thanks to colleagues at PTB for the accurate measurements and cooperation specifically during the very hot times before conferences.

I would like to thank colleagues from ASML and Carl Zeiss SMT for their support of the project and guidance in the field of industrial interest.

Dear colleagues form the nSI department, thank you for the great time! Special thanks to our ADC and MuCo engineers Frank, Santi, Bob, Arend-Jan and Peter for their enormous help with the deposition of multilayers discussed in this thesis, for their overtime work during the deposition of 100+ period multilayers and enthusiasm for work. That helps a lot!

Finally, I would like to thank my wife Natasha, for her patience during the business trips, and late hours at work, and my parents Alexander and Olga for their help and mental support!

11 Corriculum Vitae

Igor A. Makhotkin was born on 28 July 1985 in Moscow, Russia. He studied at the highschool with emphasis on mathematics and physics 444. In 2002 he started his education at the Moscow Institute of Physics and Engineering (MEPhI) in the faculty of Automatics and Electronics and after his first year he went to the Faculty of Physics of the Higher Physics College of the same Institute. During the study in MEPhI, Makhotkin followed an internship in the Institute of Crystallography, where he worked on the development of X-ray based techniques for thin film characterization. After his graduation in 2008 with the degree of specialist (old system) in the physics of condensed matter he continued working in the Institute of Crystallography. In 2009 he started his PhD work in FOM Institute for Plasma Physics Rijnhuizen, now the FOM Institute For Fundamental Energy Research DIFFER.